Interactions of Cationic Peptides and Ions with Negatively Charged Lipid Bilayers

by

Sattar Taheri-Araghi

A thesis
presented to the University of Waterloo
in fulfilment of the
thesis requirement for the degree of
Master of Science
in
Physics

Waterloo, Ontario, Canada, 2006

AUTHOR'S DECLARATION FOR ELECTRONIC SUBMISSION OF A THESIS

I hereby declare that I am the sole author of this thesis. This is a true copy of the thesis, including any required final revisions, as accepted by my examiners.

I understand that my thesis may be made electronically available to the public.

Abstract

In this thesis we study the interactions of ions and cationic peptides with a negatively charged lipid bilayer in an ionic solution where the electrostatic interactions are screened.

We first examine the problem of charge renormalization and inversion of a highly charged bilayer with low dielectric constant. To be specific, we consider an asymmetrically charged lipid bilayer, in which only one layer is negatively charged. In particular, we study how dielectric discontinuities and charge correlations among lipid charges and condensed counterions influence the effective charge of the surface. When counterions are monovalent, e.g., Na^+, our mean-field approach implies that dielectric discontinuities can enhance counterion condensation. A simple scaling picture shows how the effects of dielectric discontinuities and surface-charge distributions are intertwined: Dielectric discontinuities diminish condensation if the backbone charge is uniformly smeared out while counterions are localized in space; they can, however, enhance condensation when the backbone charge is discrete. In the presence of asymmetric salts such as $CaCl_2$, we find that the correlation effect, treated at the Gaussian level, is more pronounced when the surface has a lower dielectric constant, inverting the sign of the charge at a smaller value of Ca^{2+} concentration.

In the last chapter we study binding of cationic peptides onto a lipid-bilayer membrane. The peptide not only interacts electrostatically with anionic lipids, rearranging their spatial distributions, but it can also insert hydrophobically into the membrane, expanding the area of its binding layer (i.e., the outer layer). We examine how peptide charges and peptide insertion (thus area expansion) are intertwined. Our results show that, depending on the bilayer's surface charge density and peptide hydrophobicity, there is an optimal peptide charge yielding the maximum peptide penetration. Our results shed light on the physics behind the activity and selective toxicity of antimicrobial peptides, i.e., they selectively rupture bacterial membranes while leaving host cells intact.

Acknowledgements

I would like to take this opportunity to acknowledge those who have helped me complete this thesis. First and foremost, I would like to express my gratitude to my supervisor, Professor Bae-Yeun Ha – his encouragement, support, and thoughtful advice have been immensely valuable, both in personal and professional terms. I am particularly grateful to him for his elegant and interesting research ideas, which were the best motivations for me to work – I truly enjoyed working with him. Besides, I am indebted to other members of my defense and advisory committee, Professors Russell Thompson, Jim Davis and Chris Gray, for their constructive comments and suggestions that I found useful in improving this work. I am also grateful to Yang Li, a former member of our group – his constructive cooperation helped me a lot during the first year of my study here.

I would also like to thank my parents, to whom I would like to dedicate this thesis: my father who was the first to encouraged me to take the steps into the world of science during my high school years, and my mother whose patience has helped me pursue this journey. I would also like to thank my elder brother, Sina, who first showed me the interesting world of physics, beyond a school curriculum. His support has been so heartwarming through the years in my high school and college. I owe to him all the confidence I got to stay in physics as my professional career.

Finally, I would like to thank Natural Sciences and Engineering Research Council of Canada (NSERC) for their financial support.

This thesis is dedicated to my parents,

and my brother for all they did.

Contents

List of Figures

Chapter 1

Introduction

1.1 Biological Cells, Cell Membranes and Lipid Bilayers

Biological cells, sometimes called the *building blocks of life*, are the structural and functional units of all living organisms [1]. Some organisms, such as bacteria, are unicellular, consisting of a single cell. Other organisms, such as humans, are multicellular. The number of cells in a human body is remarkably large, about three orders of magnitude more than the number of stars in the Milky Way. However, regarding their large number, the variety of cells is much smaller: only about 200 distinct types of cells are represented in the collection of about 10^{14} cells in our body [2]. According to the cell theory, first developed in 1839 by Schleiden and Schwann, all organisms are composed of one or more cells; all cells are created by preexisting cells; all vital functions of an organism occur within cells which contain the hereditary information necessary for regulating cell functions and for transmitting information to the next generation of cells [1]. These cells have diverse capabilities and have remarkably different shapes. Simple cells, like some species of bacteria, are not much more than inflated bags. Some others, such as nerve cells, may have branched structures at each end connected by an arm that is more than a thousand times long as it is wide. The fundamental structural elements of most cells, however, are essentially the same: fluid membranes encapsulate the

cell and its components, while networks of filaments maintain the cell's shape and help organize its contents [2]. Lipid membrane, the interface between a living cell and the surrounding world, plays a critical role in numerous complex biological processes. Virus-cell fusion, peptide-bacteria interaction, exocytosis, endocytosis and ion permeation are a few examples of processes involving membranes [3].

The cell membrane is a complicated supramolecule structure that is mainly composed of phospholipids, forming a bilayer, to which proteins and other biomolecules are anchored. The phospholipids of a membrane are made of two major components: fatty acids and a phosphate group. The phosphates are the head-groups and fatty acids are the tails of the phosohplipids. Due to the polar nature of the head-groups they are attracted to the water molecules, showing hydrophilic behaviour. Non-polar tails of phospholipids, however, are not attracted to water and are said to be hydrophobic. In water, phospholipids self-assemble into a bilayer, where the hydrophobic tails line up against each other and hydrophilic head-groups are on both sides extending out into the water (Fig. 1.1). This kind of bilayer is the structural element of the membrane of the living cells. Other than biological membranes, phospholipids can also form vesicles or closed lipid bilayers extensively used in experiments. The interior and exterior of the vesicles are water that can contain different ions as well.

There are different variations of phospholipids including phosphatidyleserine (PS), phosphatidylglycerol (PG), phosphatidylcholine (PC) and phosphatidylethanolamine (PE). The head-group of some of the phospholipids are negatively charged (like PS). Incorporation of these phospholipids in a lipid bilayer results in a negative charge density for the membrane. Lipid bilayers of some cell membranes are charged at both sides, i.e., symmetrically charged. Some other cells, like red blood cells, have asymmetrically charged lipid bilayers. In these membranes, the inner layer of the bilayer is negatively charged while the outer layer is neutral. The charged layer can interact electrostatically with ions and other charged molecules near the membrane. These interactions are shown to be important in many biological processes such as lysis of bacterial membranes by antimicrobial peptides and translocation of DNA across a charged membrane [4, 5].

Many of the biomolecules are ionized in solutions. Carrying electric charge,

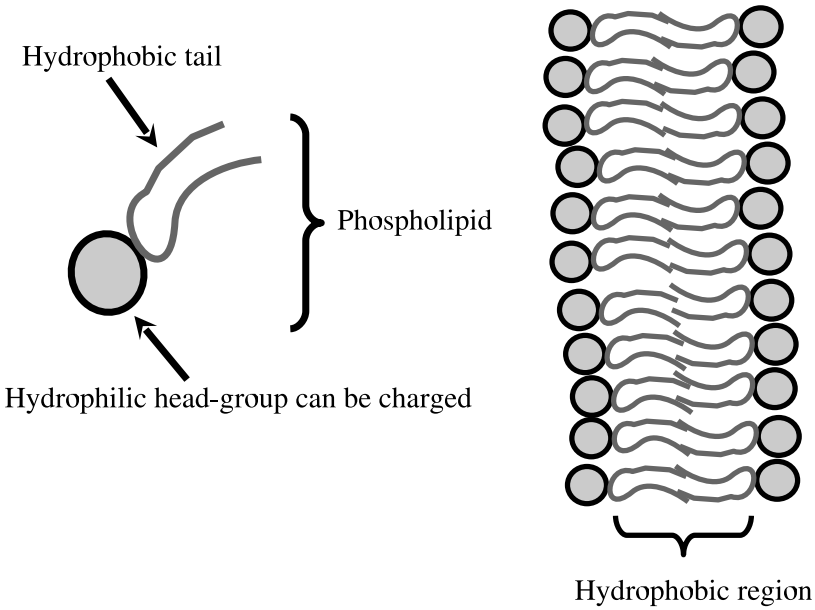

Figure 1.1: Schematic view of a phospholipid and a lipid bilayer

they can have electrostatic interaction with each other and other biomolecules. As mentioned above, these interactions can initiate important biological processes. This fact prompts us to study the details of the electrostatic interactions between charged particles in ionic solutions. Due to presence of free ions in the solution, the electrostatic interactions are screened. In the Sec. 1.3 we present a brief introduction to the physics of charge screening in ionic solutions.

1.2 Antimicrobial Peptides

Peptides are macromolecules formed by linkage of up to 50 amino acids, from a total number of 20 standard types of amino acids. Proteins have also the same primary structures. The difference proteins them and peptides is in the size of the molecule: proteins have a larger number of amino acids in their structure.

There is a large group of peptides which show antimicrobial activity against

bacteria, viruses, fungi and cancer cells. Most of these peptides have a net positive charge. There are more than 500 identified antimicrobial peptides with an average net charge of 4.54 [6]. Antimicrobial peptides are divided into four major categories: antibacterial, antiviral, antifungi and anticancer peptides; where the antibacterial peptides are the largest category among them.

The third chapter of this thesis is devoted to the interactions of antibacterial peptides with lipid bilayers.

1.3 Screening of Charged Molecules in Ionic Solutions: Poisson-Boltzmann and Debye-Hückel theories

In this section we present a brief introduction to the mean-field theories for the calculation of potentials in ionic solutions. When a charged molecule is immersed in an ionic solution, such as NaCl dissolved in water, there would be electrostatic interaction between the charged molecule with the ions in the solution. As a result of these interactions, counterions (ions which are oppositely charged to the charged molecule) are attracted and co-ions are repelled from the charged molecule. Adsorption of counterions onto the surface of the charged molecule is energetically favorable, however, this process is opposed by entropy. Ions prefer to move freely in the solution, maximizing the entropy. As the result of the competition between energy and entropy, the density of counterions would be high near the charged molecule and decreases at larger distances. In the context of equilibrium statistical mechanics, we can use the Poisson-Boltzmann equation to find the density profile of ions in the solution. According to the Boltzmann weight the probability of finding an ion of the ith kind at position $\mathbf{r}$ is exponentially related to the energy of the ion in that position. If we take only electrostatic energy into account, the energy is given by $Z_i e\psi(\mathbf{r})$, where Z_i is the valence of the ion which includes the sign of the ion, e is the electronic charge and $\psi(\mathbf{r})$ is the electrostatic potential at $\mathbf{r}$. Since the density of the ions at $\mathbf{r}$ is related to the probability of finding them at $\mathbf{r}$, we can

write

$$n_i(\mathbf{r}) \propto \exp\left(\frac{-Z_i e\psi(\mathbf{r})}{k_B T}\right). \tag{1.1}$$

where $n_i(\mathbf{r})$ refers to the density of the ions of the ith kind and $k_B T$ is the thermal energy. On the other hand, from electrostatics, we can relate the charge density to the divergence of the electric field as

$$\nabla.\left[\epsilon\nabla\psi(\mathbf{r})\right] = -4\pi\rho(\mathbf{r}) = -4\pi e\sum_i Z_i n_i(\mathbf{r}). \tag{1.2}$$

Here, $\rho(\mathbf{r})$ is the total charge density at $\mathbf{r}$ and $\sum_i$ represents the summation of all existing ions in the solution. Combination of Eqs. 1.1 and 1.2 gives the well-known Poisson-Boltzmann (PB) equation:

$$\nabla.\left[\epsilon\nabla\psi(\mathbf{r})\right] = -4\pi e\sum_i Z_i n_i \exp\left(\frac{-Z_i e\psi(\mathbf{r})}{k_B T}\right). \tag{1.3}$$

In this equation, n_i denotes the number density of the ions of the ith kind in bulk solution. When the particles in the solution are not highly charged, the electric potential is low (electric potential at infinity is assumed to be zero). In this case, the term in the exponential function would be much less than 1 and can be expanded to first order, yielding a linear differential equation for the potential known as the Debye-Hückel (DH) equation which in a space with uniform dielectric constant reads:

$$\nabla^2\psi(\mathbf{r}) = \frac{-4\pi e}{\epsilon}\sum_i Z_i n_i\left(1 - \frac{Z_i e\psi(\mathbf{r})}{k_B T}\right). \tag{1.4}$$

In the presence of monovalent and j-valent ions, the DH equation is simplified as

$$\nabla^2\psi(\mathbf{r}) = \frac{4\pi e^2}{\epsilon}\left[2n_1 + n_j Z_j(Z_j - 1)\right]\frac{\psi(\mathbf{r})}{k_B T}. \tag{1.5}$$

Here, n_1 and n_j are the densities of monovalent and j-valent ions. The particular combination of the coefficient of $\psi(\mathbf{r})$ in Eq. 1.5 is to reflect the overall electric neutrality condition (ı.e, the total charge of the system), and defines the Debye screening length, κ^{-1}, given by $\kappa^2 = 4\pi e^2\left[2n_1 + n_j Z_j(Z_j - 1)\right]/\epsilon k_B T$. The electrostatic interactions are exponentially screened at this length scale.

In the case of highly charged particles immersed in the solution, the electrostatic interaction between the charged particle and the counterions in its close proximity

is strong; some of these counterions are trapped in the vicinity of the charged particle and are referred to as *condensed counterions*. In this case, it is useful to consider the charged particle and condensed counterions as a single entity whose charge defines the *renormalized* or *effective* charge of the charged particles.

Here we should note that PB and DH theories ignore the local fluctuations of the charge densities and are thus called mean-field approaches. These density fluctuations can get important in some circumstances. As will be discussed in chapter 2 in detail, the density fluctuation can trigger more counterion condensation, which can even results in *charge inversion* under certain situations. Charge inversion is a phenomenon in which the charge of the condensed counterions exceeds the charge of the particle, in magnitude, resulting in an opposite sign for the renormalized charge of the particle with respect to its intrinsic charge. This process has been observed in the electrophoresis experiment where the direction of the movement of a charged particle in an electrolyte under applied electric field can be inverted in some situations. This can be attributed to the charge inversion since the sign of the renormalized charge determines the direction of the force on the particle. In chapter 2 we will discuss charge inversion and charge renormalization of the lipid bilayer where charge density fluctuations are incorporated in our calculations.

It is worthwhile to note that the thickness of a lipid bilayer is approximately 40Å. The dielectric constant of the phospholipid tails, the major part of the bilayer, is 2 (in Gaussian units) which is much smaller than that of the surrounding water ($\approx$ 80). In this thesis, we show that the dielectric discontinuities in the water and lipid bilayer systems play an important role in controlling the electrostatic interactions of the bilayer with ions and charged molecules around the bilayer. The effects of these discontinuities can be explained using an *image charge* method.

In electrical systems, effects of dielectric discontinuities can be accounted for image charges. According to this method, the effects of dielectric discontinuities are mimicked by image charges. The main advantage is that the dielectric constant of the resulting system (including the image charges) becomes uniform. In case of one single flat dielectric discontinuity (two semi-infinite plate with different dielectric constants attached to each other), the image charge of one particle is on the other side and the same distance from the interface. The sign and magnitude of this image

charge is, however, dependent on the dielectric constants of the dielectric media. If the charged particle is exactly on the interface between two plates, the image charge would be at the same position as the charged particles. In case of more dielectric discontinuities, like a dielectric plate in a solution where two parallel dielectric discontinuities emerge in the system, the image charges would be complicated. In this case electric fields are reflected over and over again so that there would be infinite number of image charges. Free ions, like salt ions, in the solution can make this picture even more complicated since the image charge of each ion should be taken into account. In chapter 2 and 3 of this thesis, in order to solve for the electric potentials in the system we take dielectric discontinuities explicitly into account, ı.e, we do not use image charge method. To explain special features of our results, however, our description relies on the image charge approach.

1.4 Overview of this thesis

In this thesis we study the interactions of a charged lipid bilayer with ions and cationic peptides. The thesis has two main parts: chapter 2 is focused on the charge renormalization of a highly charged lipid bilayer immeresed in an ionic solution; chapter 3 is concerned with the binding of peptides on the lipid bilayer where they can be adsorbed on the surface or penetrated inside the bilayer.

In chapter 2, we reexamine the problem of charge renormalization and inversion of a highly charged surface of a low dielectric constant immersed in ionic solutions. To be specific, we consider an asymmetrically charged lipid bilayer, in which only one layer is negatively charged. In particular, we study how dielectric discontinuities and charge correlations among lipid charges and condensed counterions influence the effective charge of the surface. When counterions are monovalent, e.g., Na^+, our mean-field approach implies that dielectric discontinuities can enhance counterion condensation. A simple scaling picture shows how the effects of dielectric discontinuities and surface-charge distributions are intertwined: Dielectric discontinuities diminish condensation if the backbone charge is uniformly smeared out while counterions are localized in space; they can, however, enhance condensation when the backbone charge is discrete. In the presence of asymmetric salts such as

$CaCl_2$, we find that the correlation effect, treated at the Gaussian level, is more pronounced when the surface has a lower dielectric constant, inverting the sign of the charge at a smaller value of Ca^{2+} concentration.

In chapter 3, we study the adsorption and penetration of antimicrobial peptides onto the surface of a fluid bilayer, composed of neutral and charged phospholipids, in an ionic solution. Using a three state model, in which peptides can be in one of the states of *free* in bulk, *adsorbed* on the bilayer's surface or *penetrated* inside the bilayer, we find the density of peptides in each state by balancing their chemical potentials. To find the free energy and chemical potentials, the non-linear Poisson-Boltzmann equation is solved self-consistently with the boundary conditions on the surface of the bilayer. These boundary conditions are determined from the local fraction of charged lipids (to all lipids) which reflects the mobility of the lipids. We find that depending on the bilayer's average charge density and hydrophobicity of the peptides there is an optimal peptide charge which yields the maximum binding affinity. We also observe a transition in the surface adsorbed and penetrated peptide populations at certain values of free peptide concentration depending on the hydrophobicity of the peptides and average surface charge density of the bilayer.

Chapter 2

Charge Renormalization and Inversion of a Highly Charged Lipid-Bilayer

2.1 Introduction

Macromolecules such as DNA and biomembranes carry a large number of charges in aqueous solution interacting with other ions. They can thus trap oppositely charged ions (counterions) in their close proximity under a variety of conditions; some of them are irreversibly adsorbed onto the surface forming the so called stern layer, but others are less tightly bound to the surface, forming a diffusive layer of excess counterions [7, 8]. While permanently adsorbed ions in the Stern layer can be considered as part of surface charges, the diffusive layer is a dynamic structure, constantly exchanging ions with those in bulk. Nevertheless, it has proven to be useful to consider the macroion and its diffusive layer as forming a single object, which is often referred to as a "dressed ion" [9, 10]. It has long been recognized that counterions in the diffusive layer play an important role in regulating the charge properties of macroions as in the electrostatic binding and transport of macroions [11–13]. It is thus of practical importance to study how their physical properties can be controlled by experimentally accessible parameters such as ionic

strength, ion valences, and dielectric properties.

In this chapter, we study the (reversible) electric binding of counterions onto an oppositely charged surface in aqueous solution. To be specific, we consider a negatively-charged lipid bilayer of thickness d and a dielectric constant $\epsilon_<$, immersed in electrolyte solutions of a dielectric constant $\epsilon_>$, as illustrated in Fig. 2.1. (The subscripts $>$ and $<$ are to remind that $\epsilon_>$ is typically larger than $\epsilon_<$.) The bilayer is assumed to be asymmetrically charged: one of the layers is negatively charged with a charge density $-e\sigma_0$ and the other one is neutral (as in red blood cell membranes [14]). In addition to monovalent salts (e.g., NaCl), there can be $Z:1$ salts (e.g., $CaCl_2$). The charged surface (at $x = 0$) can attract counterions (e.g., Na^+ or Ca^{2+}) and trap them in close proximity. This phenomenon, often referred to as counterion condensation, results in a renormalization of the surface charge [7,8]. Under certain conditions, the sign of the renormalized charge can be inverted; this phenomenon is known as "charge inversion" [15–17].

In particular, we study how dielectric discontinuities influence the electric binding of counterions or simply counterion condensation (thus charge inversion). Our main focus will be laid on the computation of renormalized charges rather than on the detailed structure of the diffusive layer. We first tackle this problem at the meanfield level. To this end, we use two seemingly-distinct methods: a two-state model [7,8] and a matching method [18]. In the latter case, the Poisson-Boltzmann (PB) equation is matched, at large distances, with the corresponding Debye-Hückel (DH) equation (or the linearized PB equation) with a renormalized charge [18]. Both approaches, in good agreement with each other, suggest that the dielectric discontinuities enhance counterion condensation for $0 < d < \infty$; as $d \to \infty$, however, the effect of dielectric discontinuities becomes irrelevant at the meanfield level as is also expected from Gauss's law (see the relevant discussion in Sec. 2.2).

Using a simple physical picture, we also examine the effect on counterion condensation of charge correlations and backbone-charge distributions. Interestingly, we find that the planar distribution of backbones charges can play an important role: The effect of dielectric discontinuities or image charges depends on how backbone charges are treated (see Sec. 2.2.1 for details). When the backbone charge is assumed to be smeared out uniformly, then the image charge weakens the attrac-

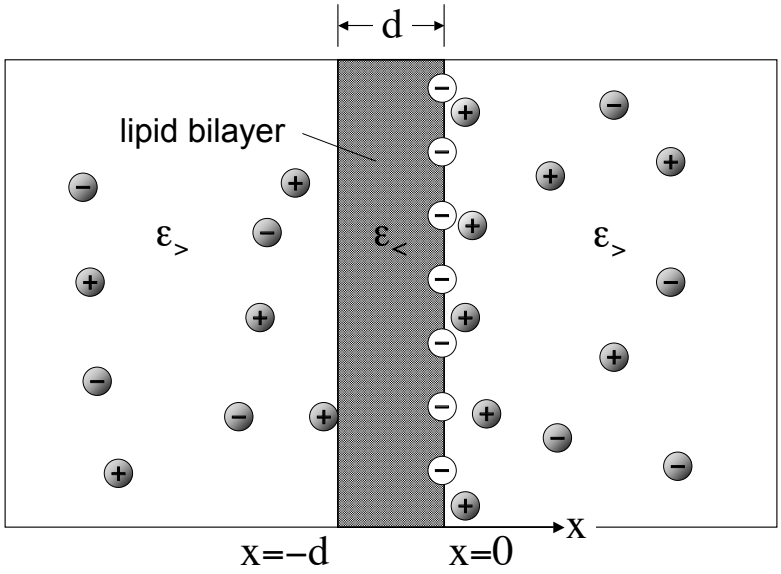

Figure 2.1: Schematic view of a negatively-charged lipid bilayer of thickness d immersed in an ionic solution. The dielectric constant of the bilayer $\epsilon_<$ is typically smaller than that of the solution $\epsilon_>$. The bilayer is assumed to be asymmetrically charged: the left side of the plate at $x = -d$ is neutral while the other side at $x = 0$ is negatively charged with a charge density $-e\sigma_0$. The resulting system resembles an asymmetrically-charged cell membrane (e.g., red blood cell membranes).

tion of counterions to the surface. When both backbone charges and counterions are treated on an equal footing, the image charge can enhance condensation.

Finally, we examine the effect of charge correlations by treating both condensed counterions and backbone charges on equal footing. To this end, we incorporate correlations at the Gaussian level within the two state model. In the presence of $CaCl_2$ (or $Z:1$ salts, $Z>1$), the (renormalized) charge of a highly charged surface is inverted (when correlations are included), consistent with previous results [15–17]. Interestingly, we find that the correlation effect is more pronounced when the dielectric constant of the surface is lower than in the solution, i.e., $\epsilon_> > \epsilon_<$, as is often the case. As a result, charge inversion can take place in wider parameter spaces – in this case, the onset of charge inversion takes place at a lower Ca^{2+} concentration than expected from the case $\epsilon_> = \epsilon_<$.

Sections of this chapter are organized as follows: Sec. 2.2 describes charge renormalization at the meanfield level; to this end, a few different versions of meanfield theory are adopted and compared. Sec. 2.3 is devoted to examining the effect of charge correlations on charge renormalization; a particular emphasis is on the interplay between charge correlations and dielectric discontinuities.

2.2 Mean-field theory

2.2.1 The Poisson-Boltzmann approach and the matching method

At the meanfield level, the spatial distribution of counterions is described by the PB (Poisson-Boltzmann) equation. The PB equation relates the electric potential $\psi(\mathbf{r})$ to the total charge density $\rho(\mathbf{r})$, where $\mathbf{r}$ is the position vector. If $n_i(\mathbf{r})$ is the number density of ions of the ith kind and valence Z_i, it follows

$$n_i(\mathbf{r}) = n_i \exp\left[-\frac{Z_i e\psi(\mathbf{r})}{k_B T}\right], \tag{2.1}$$

where e is the electronic charge, k_B the Boltzmann constant, T the temperature, and finally n_i is the bulk concentration of each species. Below we use n_i and

[ith species] interchangeably, where [ith species] is the bulk concentration of the ith species: [Na^+] is, for example, the bulk concentration of Na^+. Obviously the total charge density is given by $\rho(\mathbf{r}) = e\sum_i Z_i n_i(\mathbf{r})$. The PB equation then reads [19]

$$\nabla \cdot [\epsilon(\mathbf{r})\nabla\psi] = -4\pi\rho(\mathbf{r}) = -4\pi e \sum_i Z_i n_i \exp\left[-\frac{Z_i e\psi(\mathbf{r})}{k_B T}\right]. \tag{2.2}$$

Note that this equation is written in Gaussian units (we adopt Gaussian units throughout this thesis). Dielectric discontinuities can be taken into account through a spatially varying dielectric constant $\epsilon(\mathbf{r})$.

Without loss of generality, the surface is assumed to be aligned perpendicular to the x axis (Cf. Fig. 2.1). At the meanfield level where the local fluctuation of the ions are ignored, the system is essentially one dimensional due to the translational symmetry in y and z directions. In other words, $\psi(\mathbf{r})$ and $\rho(\mathbf{r})$ are functions of x only: $\psi = \psi(x)$ and $\rho = \rho(x)$.

In the matching method, we find a renormalized or an effective charge by matching solutions of the DH (Debye-Hückel) equation, with a renormalized charge, and those of PB equations at large distances from the surface. In other words, the PB approach maps onto the corresponding DH approach with the bare charge replaced by an effective charge. A simple result for the effective charge density $-e\sigma^*$ can be obtained for sufficiently large σ_0 in the limit $d \to \infty$, i.e., a semi-infinite plate (occupying the space $x < 0$) in contact with 1 : 1 electrolytes, i.e., NaCl: It was shown that $\sigma^* = \frac{\kappa}{\pi\ell_B}$, independent of σ_0 [20]. Here and in what follows, $\ell_B = e^2/\epsilon_> k_B T$ is the Bjerrum length, a length scale at which the electrostatic interaction between two charges becomes comparable to the thermal energy $k_B T$ (≈ 7.1Å at room temperature in water) and $\epsilon_>$ is the dielectric constant of the solvent (i.e., water); the Debye length κ^{-1} is related to ion concentrations through $\kappa^2 = 4\pi\ell_B([Na^+]+[Cl^-])$. Finally, the dielectric constant of water at room temperature is known to be 80. The electrostatic interaction is thus significantly lower in water than in a vacuum.

2.2.2 Two-state model

In a more analytical treatment, we use a two-state model, in which ions are classified as either "free" or "condensed" (i.e.,, those trapped near the surface). If $Z_i e\sigma_i$ is the

planar charge density of condensed counterions of the ith type, the effective charge density of the surface is then $-e\sigma^* = -e(\sigma_0 - \sigma_1 - Z\sigma_2)$, where the subscripts 1 and 2 refer to monovalent and Z-valent counterions, respectively. Even though we consider only monovalent ions in this section (ı.e., $\sigma_2 = 0$), we include Z-valent counterions for later convenience (Cf. Sec. 2.3). The amount of condensed counterions can be obtained by balancing chemical potentials of condensed and free counterions. The chemical potential of free ions is mainly associated with the configurational entropy of mixing: $\mu_i^{free} \simeq k_B T \ln(n_i v_0)$, where v_0 is the volume of counterions assumed to be the same for all counterions. The chemical potential of condensed counterions arises from electrostatic interactions and the entropic penalty for condensation. If $\mathcal{F}_{elec}$ is the electrostatic free energy of the charged surface per area, then the electrostatic chemical potential of condensed counterions of the ith kind is $\mu_i^{cond} = \partial \mathcal{F}_{elec}/\partial \sigma_i$.

The electrostatic free energy of a surface of a planar density $-e\sigma^*$ is simply $\frac{1}{2}\int(-e\sigma^*)\psi_0 dS$, where ψ_0 is the electrostatic potential evaluated at the surface and dS is a surface element. At the DH level (with a renormalized surface charge σ^*), the electrostatic free energy per unit area is simplified as $\mathcal{F}_{elec} = \frac{1}{2}(-e\sigma^*)\psi_0$, since the charge distribution is assumed to be uniform over the surface. We calculate ψ_0 by solving DH equation which is described in details in Appendix A (Cf. Eq. ($A4$)). We find that for $\kappa^{-1} \gg \ell_c$ [21]

$$\begin{aligned} \mathcal{F}_{elec} &= \frac{1}{2}(-e\sigma^*)\psi_0 \\ &= k_B T \times 2\pi\sigma^{*2}\,\kappa^{-1}\ell_B \frac{(\epsilon_< + \epsilon_> \kappa\, d)}{(2\epsilon_< + \epsilon_> \kappa d)}, \end{aligned} \tag{2.3}$$

where $\epsilon_<$ and $\epsilon_>$ are dielectric constants of the bilayer and the solvent, respectively, and κ^{-1} is the Debye screening length given by $\kappa^2 = 4\pi\ell_B[2n_1 + Zn_2(Z+1)]$ with n_1 and n_2 the bulk concentration of monovalent and Z-valent ions, respectively. We thus have

$$\frac{\mu_i{}^{cond}}{k_B T} = -4\pi Z_i \sigma^* \kappa^{-1}\ell_B \frac{(\epsilon_< + \epsilon_> \kappa d)}{(2\epsilon_< + \epsilon_> \kappa d)} + \ln\left(\frac{\sigma_i v_0}{\ell_c^i}\right), \tag{2.4}$$

where ℓ_c^i is the thickness of the condensed layer. The second term in Eq. (2.4) corresponds to the entropic penalty for confining counterions in a layer of thickness ℓ_c^i.

Despite its simplicity, the two state model suffers a drawback: there can be ambiguity in choosing the thickness of condensed layers ℓ_c (the superscript i was dropped). In the past, ion sizes were often chosen as ℓ_c [7, 8]. While this sounds reasonable, it is not clear whether this choice will lead to σ^* consistent with the matching method. For a semi-infinite plate ($d \to \infty$) in a 1 : 1 electrolyte, the two approaches can easily be reconciled by mapping the two state model onto the matching method. In other words, we equate $\sigma^* = \frac{\kappa}{\pi \ell_B}$ with σ^* obtained from the two state model. By noting that $\sigma_1 \approx \sigma_0$ for large σ_0 (this is also the condition under which $\sigma^* \approx \frac{\kappa}{\pi \ell_B}$), we find

$$\ell_c \approx \left(\frac{\kappa^{-2}}{\lambda}\right)\left(\frac{4}{\exp(4)}\right), \tag{2.5}$$

where $1/\lambda = 2\pi \ell_B \sigma_0$. Note that this is valid only when $\kappa^{-1} \gg \ell_c$; see the relevant discussion in endnote [21]. This result indicates that ℓ_c increases quadratically with κ^{-1}. As a result, ℓ_c can be much larger than the Gouy-Chapmann length λ. For finite d, dielectric discontinuities will be reflected in ℓ_c. On the other hand, this will not sensitively influence σ^*, since σ^* varies logarithmically with ℓ_c. In this case, Eq. (2.5) is expected to be a good approximation for a wide range of parameters (also see Fig. 2.2). The two-state model and the matching method can thus be used interchangeably. For typical values of parameters ($\lambda \sim 10$Å, $\kappa^{-1} \sim 10{-}100$Å), ℓ_c is smaller than typical ion sizes $a_0 \sim 5$Å. It is thus natural to choose $\ell_c \sim a_0$ (Cf. Figs. 2.3 & 2.5).

2.2.3 Dielectric discontinuity

To test ℓ_c in Eq. (2.5) in the presence of dielectric discontinuities, we have calculated σ^* of the charged surface (at $x = 0$) using the two state model, with ℓ_c determined by Eq. (2.5), and the matching method. We have plotted σ^* as a function of σ_0 for a few different choices of κ (see Fig. 2.2). We have chosen $d = 4$nm, $\epsilon_> = 80$, $\epsilon_< = 2$, and $T = 300$K. In the figure, two state model and the matching method are described by the dotted and the solid lines, respectively. The agreement between the two approaches is excellent. This justifies our expression for ℓ_c in Eq. (2.5)

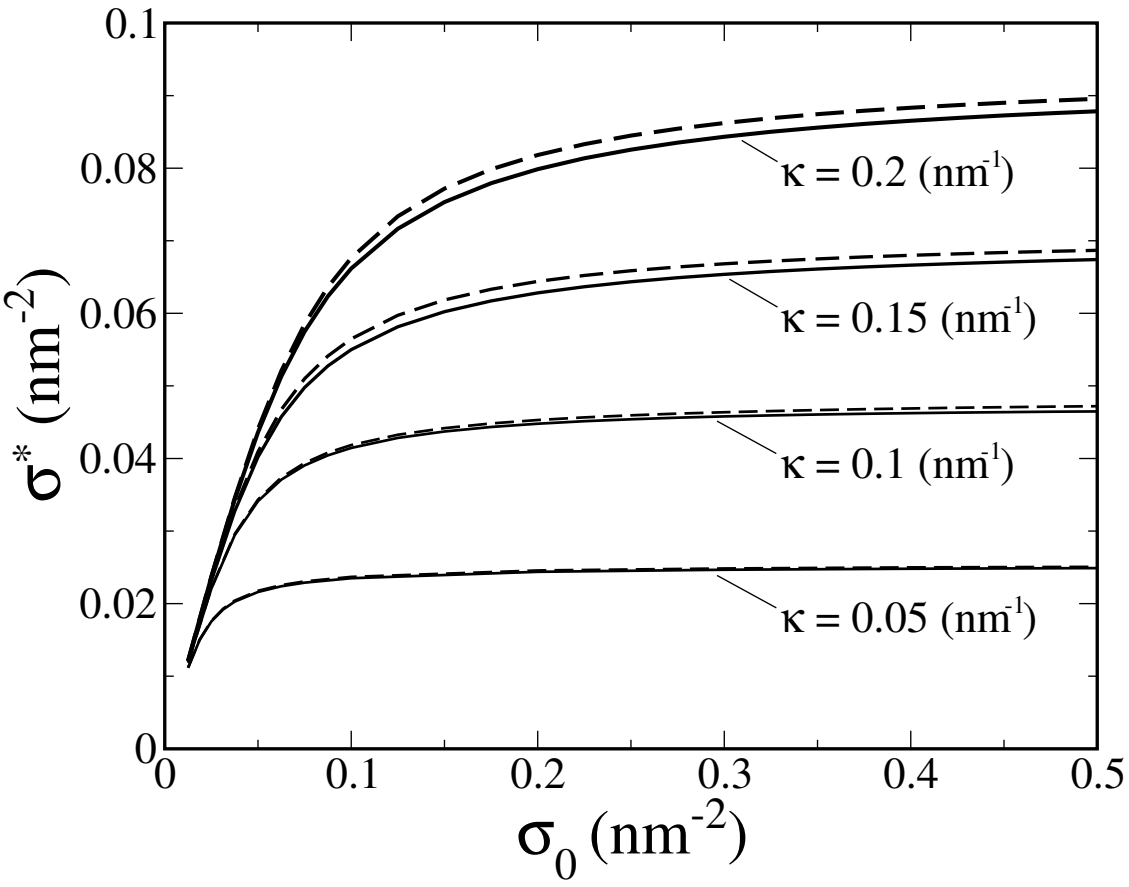

Figure 2.2: Effective planar density σ^* obtained from the two state model (the dashed line) and the matching method (the solid line). We have chosen $d = 4$nm, $\epsilon_> = 80$, $\epsilon_< = 2$, and $T = 300$K; in two-state model calculations, ℓ_c has been determined by Eq. 2.5, which was originally obtained for the limit $d \to \infty$ (or $\kappa d \to \infty$). The two approaches are in good agreement with each other, implying that ℓ_c in Eq. (2.5) is valid for a wide range of κd (even when dielectric discontinuities are allowed.)

for a wide range of $\epsilon_<$ (thus d as well), even though it was originally obtained for $d \to \infty$.

For an asymmetrically-charged bilayer of finite thickness d, it is useful to examine counterion distributions on both sides of the bilayer. For simplicity we limit ourselves to monovalent cases, i.e., a bilayer immersed in an NaCl solution. We have used the two-state model to calculate the planar density of condensed counterions σ_1; the effective planar densities at $x = 0$ and $x = -d$ are $\sigma^* = \sigma_0 - \sigma_1(x = 0)$ and $\sigma^* = \sigma_1(x = -d)$, respectively. The chemical potentials of counterions at the surfaces at $x = 0$ and $x = -d$ are presented in Appendix A. Using these we have calculated $\sigma_1(x = 0)$ and $\sigma_1(x = -d)$ (see Fig. 2.3) for a few different values of $\epsilon_<$; the top three curves are for the charged surface at $x = 0$, while the bottom three curves are for the neutral surface at $x = -d$. On the other hand, we have chosen $\sigma_0 = 0.2\text{nm}^{-2}$, $\epsilon_> = 80$, $T = 300\text{K}$, and $[\text{Na}^+] = 15\text{mM}$ (corresponding to $\kappa^{-1} = 2.5\text{nm}$). Finally $\ell_c \approx 4\text{Å}$ in the limit $d \to \infty$. Since $\epsilon_>\kappa d \gg \epsilon_<$ for the parameters used, $\ell_c \approx 4\text{Å}$ is a good approximation for $d = 4\text{nm}$. We have thus chosen $\ell_c = a_0 = 5\text{Å}$ (ℓ_c cannot be smaller than the ion size $a_0 \approx 5\text{Å}$). As shown in the figure, σ_1 tends to get saturated for large d in an $\epsilon_<$-dependent way; smaller d is required for smaller $\epsilon_<$ in a κ-dependent way. (The κ dependence of saturation is not shown in the figure but can be inferred from Eq. (2.4). What matters is this combination: κd.) Also note that $\sigma_1(x = -d)$ tends to a finite value, $\sigma_1^\infty = \lim_{d\to\infty} \sigma_1 \approx 0.005\text{nm}^{-2}$, as d increases. This is a bit puzzling, since the attraction of counterions to the surface at $x = -d$ is minimal for $\epsilon_>\kappa d/\epsilon_< \gg 1$, implying that $\sigma_1^\infty \simeq 0$. As it turns out, σ_1^∞ (> 0) reflects $[\text{Na}^+]$, i.e., the bulk Na^+ concentration: $\sigma_1^\infty/\ell_c = [\text{Na}^+]$. In other words, the Na^+ concentration is uniform in the region $x < -d$, meaning that there is no condensation. For typical values of d ($\simeq 4\text{nm}$) and $\epsilon_<$ ($\simeq 2$), counterion condensation mainly takes place on the charge surface: $\sigma_1(d = 4\text{nm}) \approx \sigma_1^\infty$. In what follows, we ignore condensation on the neutral surface.

Our results in Fig. 2.3 indicate that dielectric discontinuities can enhance counterion condensation for $0 < d < \infty$. In the limit $d \to \infty$, however, the dielectric properties of the plate are not felt by counterions. This is not surprising: Our two state model in this section suppresses charge fluctuations. In this case, Gauss's law

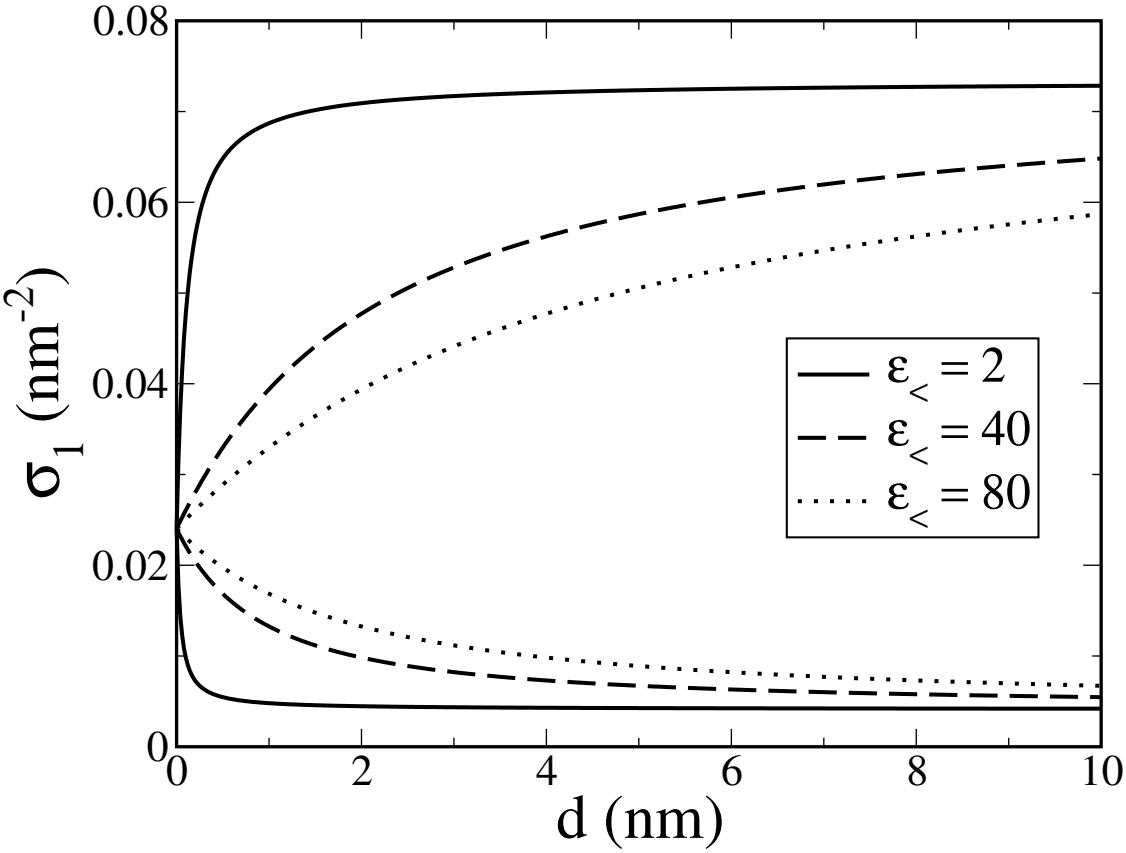

Figure 2.3: Planar density of condensed counterions obtained from the two-state model at the charged and neutral surface. We have chosen $\sigma_0 = 0.2\text{nm}^{-2}$, $\epsilon_> = 80$, $T = 300\text{K}$, $\ell_c = 5\text{Å}$, and $[\text{Na}^+] = 15\text{mM}$ (thus $[\text{Cl}^-] = 15\text{mM}$). The top (bottom) three curves correspond to the charged (neutral) surface at $x = 0$ ($x = -d$). Note that σ_1 becomes d independent for $\kappa d\epsilon_>/\epsilon_< \gg 1$ (shown clearly in the figure only for $\epsilon_< = 2$) – in this case, condensation on the neutral surface is minimal and can be ignored (see the text for details).

indicates that the electric field cannot penetrate the plate. In other words, the electric field vanishes for $x < 0$ independently of $\epsilon_<$, as also implied by Eq. $(A4)$ in the limit $d \to \infty$. This accounts for the $\epsilon_<$ independence of σ_1 in the limit $d \to \infty$. Not surprisingly, the effect of the dielectric discontinuity becomes minimal as $d \to 0$.

To augment our finding of $\epsilon_<$-dependent σ_1, we have solved the PB equation (Cf. Eqs. 2.1 and 2.2) for a few different choices of $\epsilon_<$ and plotted our results for $n_+(x)$ $(= [\mathrm{Na}^+](x)$, i.e., Na^+ concentration at $x)$ in Fig. 2.4. To this end, we have used essentially the same boundary conditions adopted in Appendix A (see Eqs. $(A3.1)$-$(A3.3)$), except that Eq. $(A3.3)$ has been approximated by $\psi(x) = 0$ at $x = 25\kappa^{-1}$. We have chosen $d = 40$Å, $\epsilon_> = 80$, $T = 300$K, and $[\mathrm{Na}^+] = 1$mM. As shown in the figure, $n_+(x)$ near the surface is larger for $\epsilon_< = 2$ than for $\epsilon_< = 80$. Our results suggest that counterion condensation can be more pronounced for smaller values of $\epsilon_<$ (as long as d is not too small or too large), in accord with the results in Fig. 2.3 – note that this happens when $\epsilon_< < \epsilon_>$, as is the case for a lipid bilayer immersed in water.

Our meanfield results in Figs. 2.3 & 2.4 suppress charge correlations and are expected to work well for low charge densities or at high temperatures. In the next section, we study how charge correlations can influence counterion condensation.

2.3 charge correlations

2.3.1 scaling theory: unscreened cases

The meanfield approach in the last section indicates that the effect of dielectric discontinuities becomes irrelevant in the limit $d \to \infty$. This appears to be distinct from those discussed in Refs. [15,16,22,23], which seem to indicate that counterion condensation is diminished by image charges in this limit. It is tempting to attribute the seeming discrepancy to charge correlations which are suppressed in our meanfield calculations. In this subsection, we use simple arguments to discuss the potential effect on counterion condensation of charge correlations and backbone-charge distributions.

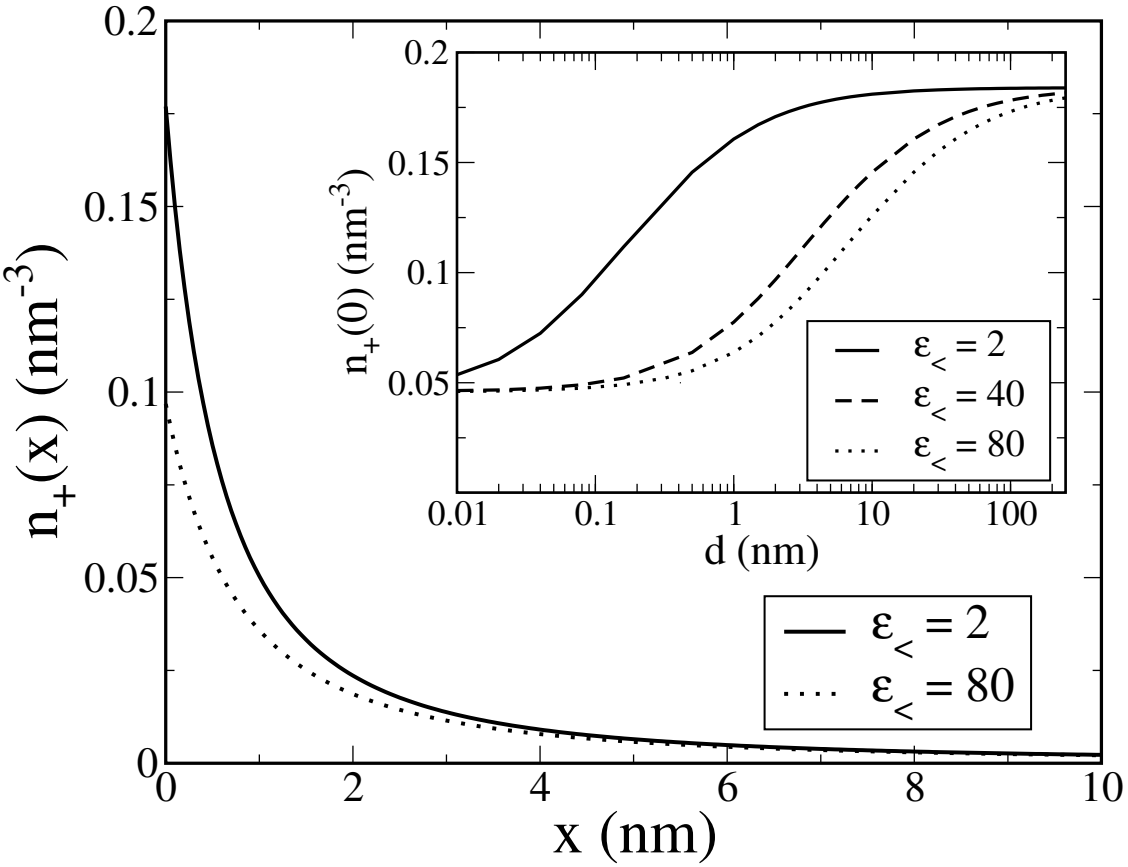

Figure 2.4: Spatial distribution of counterions near the charged surface in an ionic solution for different choices of $\epsilon_<$, obtained from the Poission-Boltzmann equation. We have chosen $\epsilon_> = 80$, $\sigma_0 = 0.2\text{nm}^{-2}$, $d = 4\text{nm}$, $T = 300\text{K}$, and $[\text{Na}^+] = 1\text{mM}$. These results indicate that the dielectric discontinuities at $x = 0$ and $x = -d$ enhance counterion condensation at the charged surface ($x = 0$). In the limit $d \to \infty$ or $d \to 0$, however, the effect of the dielectric discontinuity becomes minimal (see the inset).

Following Refs. [16,24], in the limits $\kappa \to 0$ and $d \to \infty$, the electrostatic energy of a single (monovalent) counterion at $\mathbf{r} = (x, y, z)$ due to surface charges at $\mathbf{R}_\alpha$ and its image charge is given by

$$\frac{u(\mathbf{r})}{k_B T} = -\ell_B(1+\Delta)\sum_\alpha \frac{1}{|\mathbf{r}-\mathbf{R}_\alpha|} + \frac{\ell_B \Delta}{4x}, \tag{2.6}$$

where $\Delta = (\epsilon_> - \epsilon_<)/(\epsilon_> + \epsilon_<)$. In the continuum limit (ı.e., backbone charges are smeared out), $u(\mathbf{r})$ becomes

$$\frac{u(x)}{k_B T} = 2\pi(1+\Delta)\ell_B \sigma_0 x + \frac{\ell_B \Delta}{4x}. \tag{2.7}$$

Not surprisingly, $u(x)$ has a minimum at a finite value of $x = x_{min}$:

$$x_{min} = \sqrt{\frac{\Delta}{8\pi(1+\Delta)\sigma_0}}. \tag{2.8}$$

The minimum electrostatic energy is then given by

$$\frac{u_{min}}{k_B T} = \ell_B \sqrt{\Delta(1+\Delta)\sigma_0}. \tag{2.9}$$

Clearly, u_{min} increases as Δ increases, implying that counterion condensation is diminished by the dielectric jump at the interface $x = 0$. This contradicts the PB approach which implies that a single dielectric discontinuity does not affect spatial distributions of counterions for $d \to \infty$.

The reasoning leading to Eq. (2.9) is that the backbone charge is smeared out uniformly while the counterion is localized in space. To see the potential effect of backbone-charge distributions more clearly, let's consider only one backbone charge at the origin interacting with a counterion on the x axis. Eq. (2.6) then reduces to

$$u_1(x) = -\ell_B(1+\Delta)\frac{1}{x} + \frac{\ell_B \Delta}{4x} = -\ell_B\left(1 + \frac{3\Delta}{4}\right)\frac{1}{x}. \tag{2.10}$$

Interestingly, this is more attractive for larger Δ in contrast to what we would expect from Eq. (2.9) obtained in the continuum limit.

Neither Eq. (2.7) nor Eq. (2.10) does not necessarily represent our system accurately. First, both backbone charges and counterions are mobile (with the former

confined to a surface) and can contribute to correlations. They thus have to be treated on equal footing. Furthermore, these equations are based on a one-particle picture, a single counterion interacting with a surface in the former and a counterion interacting with a backbone charge in the latter. "Many-body effects" (e.g., counterion-counterion interactions) can complicate the picture.

Another extreme case that goes beyond the one-particle description amounts to picturing backbone charges and counterions as forming a two dimensional ordered (crystalline) structure on a square lattice of a lattice constant a at the water-plate interface. An anion is then surrounded by four nearest-neighbor cations and a cation by four nearest-neighbor anions. Clearly the energy of the resulting system (per ion) is proportional to $\ell_B(1+\Delta)$

$$\begin{aligned} \frac{u_{min}}{k_BT} &= -\frac{\ell_B}{a}(1+\Delta)\left(-4+\frac{4}{\sqrt{2}}+\frac{4}{2}-\frac{8}{\sqrt{5}}+...\right) \\ &\approx -\frac{\ell_B}{a}(1+\Delta)\times 1.14. \end{aligned} \tag{2.11}$$

This is more negative for larger Δ. In this simple picture, counterions are more strongly attracted to the surface when $\epsilon_< < \epsilon_>$, implying that condensation is enhanced by the dielectric jump at the interface.

This calculation is complimentary to our meanfield approach. If the former is relevant for high electrostatic couplings, the latter is suitable for low couplings. A simpler version of the PB approach is a capacitor model in which the double layer is approximated by a parallel capacitor: a negatively charged plate at $x=0$ and a positively charged layer at $x=\delta$. In the limit $d\to\infty$, the image charge of the former (per area) located at $x=0$ is $-e\Delta\sigma_0$, which adds to the backbone charge $-e\sigma_0$, while the image charge of the latter (per area) located at $x=-\delta$ is $e\Delta\sigma_0$. The total electric field felt by the counterion layer at $x=-\delta$ is

$$E_x = \frac{4\pi e}{\epsilon_>}\left[\Delta\sigma_0-(1+\Delta)\sigma_0\right] = -\frac{4\pi e}{\epsilon_>}\sigma_0. \tag{2.12}$$

This is independent of Δ and accounts for our earlier finding that counterion condensation is not influenced by image charges in the limit $d\to\infty$. Clearly, we need to include correlations to see the effect of image charges on counterion condensation in that limit.

Our simple arguments presented in the last few paragraphs suggest that the effect of dielectric discontinuities on counterion condensation depends on how we treat backbone charges and counterions. This is indeed consistent with a recent paper by Moreira and Netz [24], which shows how surface-charge modulation is intertwined with dielectric discontinuities (also see Netz [25]). The effect of image-charge repulsions is strongest when the surface charges are assumed to be uniformly smeared out, as also implied by Eq. (2.7). As a result, the spatial distribution of counterions has a peak at a finite separation from the surface (reminiscent of x_{min} in our Eq. (2.7)). As the surface charge distribution becomes more heterogeneous for a given total surface charge, however, the peak moves towards the surface: x_{min} is diminished (see their Fig. 4b for details) as also implied by our simple scaling analysis. When coupled to correlations, the dielectric jump at the water-bilayer interface can enhance counterion condensation (even in the limit $d \to \infty$).

For a weakly to a moderately highly charged surface, surface charges (both backbone charges and condensed counterions) can be driven by thermal fluctuations, which diminish their lateral ordering. In that case, it is reasonable to consider them as forming a two dimensional ionic fluid, as compared to a two-dimensional crystal. In the next section, we develop two-dimensional DH theory of such an ionic fluid to account for correlations. The resulting approach is distinct from existing approaches [15, 16, 22, 23] in that we treat both backbone charges and counterions on equal footing and consider them as fluctuating objects.

2.3.2 Charge correlations and charge inversion

The previous subsection illustrates the interplay between charge correlations and dielectric discontinuities in determining u_{min}, the minimum electrostatic energy of a counterion near and at an oppositely charged surface. Here, we study how charge correlations can influence counterion condensation. A number of theoretical approaches suggest that charge correlations between condensed counterions (of high valency) can trigger extra condensation, leading to "charge inversion" of a highly-charged surface [15–17]. In these approaches [15–17], condensed counterions are considered as forming a strongly correlated liquid on the background of

uniformly-distributed backbone charges. As evidenced in Subsec. III.A, backbone-charge distributions can have a nontrivial effect on counterion condensation. In our approach, we treat both backbone charges and condensed counterions on equal footing as fluctuating objects on a plane. To this end, we incorporate in-plane charge correlations at the Gaussian level.

In order to set up an effective interaction $\phi(\mathbf{r}_\perp, \mathbf{r}'_\perp)$ between two charges e's on the surface at $x = 0$ (see Fig. 2.1), we first need to integrate out degrees of freedom associated with free ions. This can be readily done at the DH level: In the limit $d \to 0$ (the effect of dielectric discontinuities is irrelevant), this amounts to using a screened electrostatic interaction of the form: $\phi(\mathbf{r}_\perp, \mathbf{r}'_\perp) = \frac{e^2}{\epsilon_>} \frac{e^{-\kappa|\mathbf{r}_\perp - \mathbf{r}'_\perp|}}{|\mathbf{r}_\perp - \mathbf{r}'_\perp|}$. Obviously, this is the solution of $(\nabla^2 - \kappa^2)\,\phi = -(4\pi e^2/\epsilon_>)\delta(\mathbf{r}_\perp - \mathbf{r}'_\perp)$. However, the presence of dielectric discontinuities (coupled with finite thickness) can easily complicate $\phi(\mathbf{r}_\perp, \mathbf{r}'_\perp)$. The dielectric discontinuity can be incorporated through a spatially-varying dielectric constant $\epsilon(\mathbf{r})$:

$$\left[\nabla \cdot \epsilon(\mathbf{r})\nabla - \epsilon(\mathbf{r})\kappa^2(\mathbf{r})\right] \phi(\mathbf{r}, \mathbf{r}') = -4\pi e^2 \delta(\mathbf{r} - \mathbf{r}') \tag{2.13}$$

Note that the spatially varying screening length $\kappa^{-1}(\mathbf{r}) = \kappa^{-1}(x)$ is to reflect the absence of ions inside the plate (see also Appendix B).

At the DH level, the explicit form of $\phi(\mathbf{r}_\perp, \mathbf{r}'_\perp)$ can be found without further approximations. By symmetry consideration, we have $\phi(\mathbf{r}_\perp, \mathbf{r}'_\perp) = \phi(\mathbf{r}_\perp - \mathbf{r}'_\perp)$ – without loss of generality, we can set $\mathbf{r}'_\perp = 0$. In Appendix B, we have solved this equation for our system depicted in Fig. 2.1 with appropriate boundary conditions (see the appendix for details). The result is

$$\phi(\mathbf{r}_\perp) = \int \frac{d^2\mathbf{q}}{(2\pi)^2} e^{i\mathbf{q}\cdot\mathbf{r}_\perp} \phi(\mathbf{q}), \tag{2.14}$$

where $\phi(\mathbf{q})$ is the Fourier transform given by

$$\beta\phi(\mathbf{q}) = \frac{4\pi\ell_B}{\sqrt{\kappa^2 + q^2} + \eta q} \left[1 + \xi\,(\xi - 1)\,\frac{\exp(-2qd)}{1 - \xi^2 \exp(-2qd)}\right], \tag{2.15}$$

with $\beta = 1/k_B T$, $\eta = \epsilon_</\epsilon_>$ and ξ defined as

$$\xi = \frac{\epsilon_>\sqrt{\kappa^2 + q^2} - \epsilon_< q}{\epsilon_>\sqrt{\kappa^2 + q^2} + \epsilon_< q}. \tag{2.16}$$

Note that similar issues have been addressed in the literature. For example, $\phi(\mathbf{r}_\perp)$ in the limit $\kappa \to 0$ was first obtained in Ref. [26]. More recently, Netz considered electrolytes confined to a system of a slab sandwiched between two semi-infinite half spaces, whose dielectric constants can be different from each other [27]. At the Debye-Hückel level, he derived an effective Coulomb interaction between two charges (see $v_{DH}(\mathbf{r}, \mathbf{r}')$ in Eqs. (A.7)-(A.9) of Ref. [27]). One of the main differences between ϕ and v_{DH} is that the latter works for charges that are not on an interface with a dielectric jump, while the former was constructed exclusively for charges on such an interface.

At the Gaussian level, the free energy arising from in-plane charge fluctuations on the surface can be readily taken into account. If $\delta\sigma(\mathbf{r}_\perp)$ is the planar charge fluctuation (per e) at $\mathbf{r}_\perp = (y, z)$ (normal to the x axis), the Hamiltonian describing fluctuations can be written as [28]

$$\beta H_{corr} = \frac{1}{2} \int d\mathbf{r}_\perp d\mathbf{r}'_\perp \left[\frac{\delta\left(\mathbf{r}_\perp - \mathbf{r}'_\perp\right)}{\chi} + \beta\phi(\mathbf{r}_\perp - \mathbf{r}'_\perp) \right] \delta\sigma(\mathbf{r}_\perp)\delta\sigma(\mathbf{r}'_\perp), \qquad (2.17)$$

where $\chi = \sigma_0 + \sigma_1 + Z^2\sigma_2$ (and $\beta = 1/k_BT$). The first term corresponds to the entropic penalty for charge-density fluctuations. While all surface charges are taken into account explicitly through $\sigma(\mathbf{r}_\perp)$, free ions are considered as screening the interaction between surface charges and are taken into account through ϕ.

In the Fourier space $\mathbf{q}$, conjugate to $\mathbf{r}_\perp$, the Hamiltonian (per unit area) is simplified:

$$\beta\mathcal{H}_{corr} = \frac{1}{2} \int \frac{d^2\mathbf{q}}{(2\pi)^2} \left[\chi^{-1} + \beta\phi(\mathbf{q})\right] |\delta\sigma(\mathbf{q})|^2. \qquad (2.18)$$

By carrying out the Gaussian integrals with respect to $\delta\sigma(\mathbf{q})$, we find the correlation contribution to the free energy $\mathcal{F}_{corr}$ (after subtracting an appropriate "self-energy" term):

$$\beta\mathcal{F}_{corr} = \frac{1}{2} \int \frac{d^2\mathbf{q}}{(2\pi)^2} \left\{ \ln\Big[1 + \chi\beta\phi(\mathbf{q})\Big] - \chi\beta\phi(\mathbf{q}) \right\}. \qquad (2.19)$$

In endnote [29], we derive this result using the Debye-charging process. Note that the correlation free energy in Eq. (2.19) was constructed so that it vanishes as $\chi \to 0$ as it should. In practical calculations of $\mathcal{F}_{corr}$, we cut off high q values by

imposing an upper limit for the integral, which will be chosen to be 2π. On the other hand, the lower limit will be chosen to be 0.

The charge-correlation contribution to the chemical potential of condensed counterions is simply

$$\mu_i^{corr} = \frac{\partial \mathcal{F}_{corr}}{\partial \sigma_i}. \tag{2.20}$$

The total chemical potential of condensed counterions is then given as the sum of this and the one in Eq. (2.4).

We have calculated the amount of condensed counterions. In Fig. 2.5, we have plotted the effective charge density $-e\sigma^*$ as a function of $[Ca^{2+}]$, the bulk Ca^{2+} concentration in mM, for various choices of $\epsilon_<$. We have chosen $\epsilon_> = 80$, $T = 300$K, and $\sigma_0 = 0.2\text{nm}^{-2}$; we have also assumed that the system contains 100mM of monovalent ions (or $[Na^+] = 50$mM). According to Eq. (2.5), $\ell_c \approx 1.2$Å in the absence of $CaCl_2$. While it is possible to generalize Eq. (2.5) to include $Z:1$ salts, we rather invoke simplification based on the following physics ground: Unless $[Ca^{2+}]$ is too small, Ca^{2+} can be preferentially condensed onto the surface (see [30] for details). It is thus reasonable to assume that condensed counterions are mostly Ca^{2+}. In this case, we expect ℓ_c to be twice the corresponding value for Na^+ – here we assume that κ is mainly determined by Na^+. (Recall $\ell_c \propto \lambda^{-1}$ and note that λ^{-1} for $Z = 2$ is twice that for $Z = 1$.) The resulting ℓ_c is smaller than typical ionic sizes (~ 5Å). We have thus chosen $\ell_c = 5$Å. A number of interesting features emerge from the results in the figure:

First, they show that charge inversion occurs beyond a certain value of $[Ca^{2+}]$ or the onset concentration of Ca^{2+}. This finding is consistent with existing results [15–17]. The effect of charge correlations on condensation is more pronounced when the surface has lower dielectric constant, as is the case for lipid bilayers in water. As a result, charge inversion occurs for a wider range of $[Ca^{2+}]$ for smaller values of $\epsilon_<$. Interestingly, the onset concentration (of Ca^{2+}) is highly sensitive to $\epsilon_<$: When the dielectric discontinuity is suppressed ($\epsilon_< = \epsilon_>$) [31], the onset of charge inversion takes place at $[Ca^{2+}] \approx 7$mM. For $\epsilon_< = 2$, the onset concentration is ~ 0.1mM, about two orders of magnitude smaller than in the case of $\epsilon_< = \epsilon_>$.

A related point of interest is that the effect of dielectric discontinuities on con-

densation is more pronounced for large values of $[Ca^{2+}]$. This implies that dielectric discontinuities are more efficiently felt when charge correlations are included. Indeed our meanfield (MF) results, obtained with the two state model or the matching method introduced in Sec. 2.2, are much less sensitive to $\epsilon_<$. Additionally, for large values of $[Ca^{2+}]$, the corresponding meanfield (MF) results deviate appreciably from our correlation calculations. This indicates that meanfield approaches can easily break down in the presence of multivalent counterions.

2.4 Conclusions

To summarize, we have studied how the dielectric properties of a charged surface influence counterion condensation onto the surface. The Poisson-Boltzmann approach and the two-state model indicate that dielectric discontinuities enhance counterion condensation (when the surface has a low dielectric constant, as is the case for a lipid bilayer or other biomolecules in water). This finding appears to contradict earlier results [15, 16, 22, 23] that counterions are pushed away from the surface by image charges. Using simple scaling arguments, we have shown how the effect of image charges is intertwined with backbone-charge distributions. When the backbone charge is assumed to be uniformly smeared out while counterions are localized in space, the image charge tends to diminish counterion condensation [15,16,22,23]. When the backbone charge and counterions are treated on equal footing, however, image charges rather enhance counterion condensation. Finally, we have also studied charge inversion of a highly charged surface in a mixture of NaCl and $CaCl_2$ electrolytes. To this end, we have incorporated in-plane charge correlations at the Gaussian level into the two-state model. At a certain value of Ca^{2+} concentration, the sign of the surface charge is inverted, consistent with earlier results [15–17]. Interestingly, a smaller Ca^{2+} concentration is required for charge inversion when the surface has a lower dielectric constant; the dielectric discontinuity can lower the onset concentration of Ca^{2+} dramatically, indicating that the in-plane correlation is more important in the presence of dielectric discontinuities.

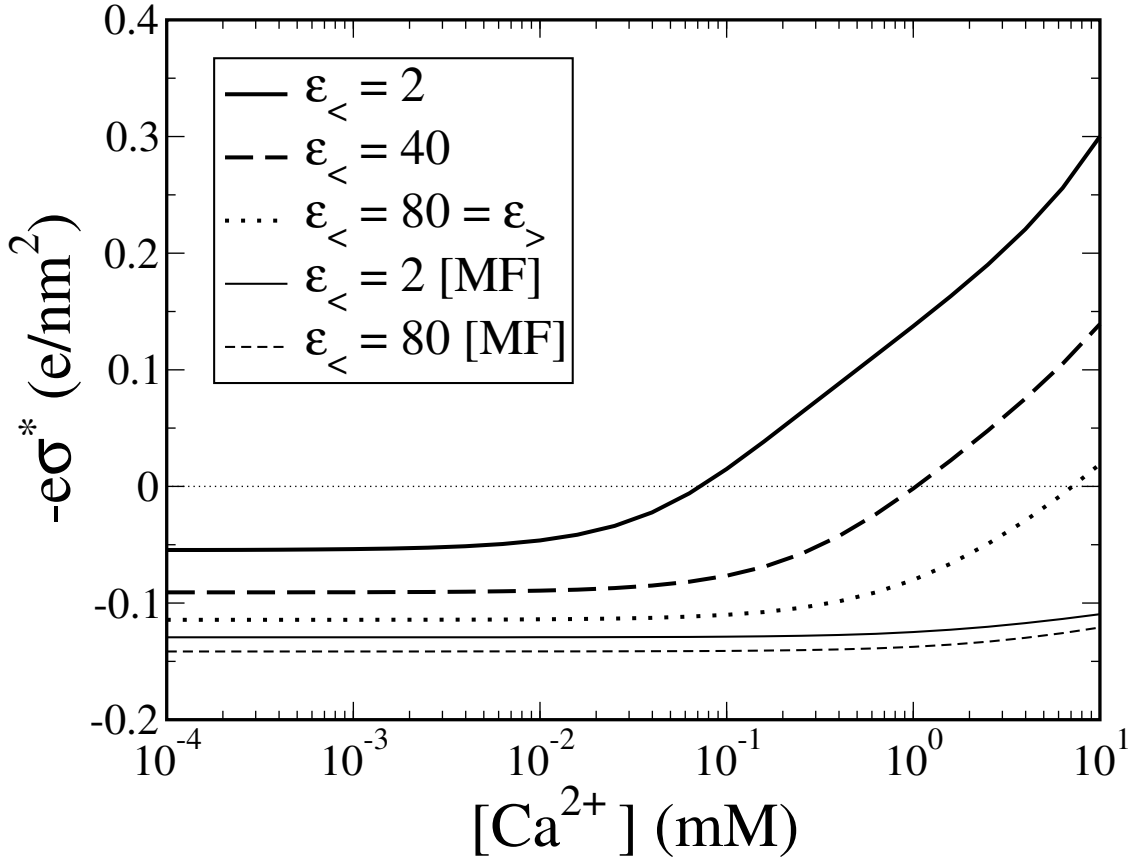

Figure 2.5: Effective planar charge density of the charged surface in the presence of 50mM of NaCl as a function of [Ca^{2+}], the bulk Ca^{2+} concentration in mM. We have chosen $-e\sigma_0 = -0.2\text{e/nm}^2$, $T = 300\text{K}$, $\ell_c = 5\text{Å}$, $d = 40\text{Å}$, and $\epsilon_> = 80$. At low Ca^{2+} concentrations, the surface is undercharged (i.e., $-e\sigma^* < 0$) but, beyond a certain concentration, it is overcharged (i.e., $-e\sigma^* > 0$). The onset concentration for overcharging is sensitive to the dielectric properties of the surface; it is smaller for a smaller value of $\epsilon_<$.

Appendix A

In this Appendix, we recapture some of our results at the Debye-Hückel (DH) level, which are relevant for low surface charge densities; we also derive chemical potentials of condensed counterions within the two-state model. Our major conclusion, i.e., enhanced counterion condensation by dielectric discontinuities, can be augmented by the DH calcualtions. To this end, we consider a dielectric plate with thickness d and dielectric constant $\epsilon_<$ immersed in an ionic solution of dielectric constant $\epsilon_>$ (typically larger than $\epsilon_<$); only one side of the plate at $x = 0$ is charged with charge density $-e\sigma$, as illustrated in Fig. 2.1. The main advantage of examining the DH limit lies in that it allows an analytically tractable analysis of the spatial distribution of counterions. Our DH calculations will thus test more elaborate results reported in the main text. We show that, as $\epsilon_< \to \epsilon_>$, the density of counterions reduces near and at the charged surface and increases around the neutral surface. Of course the entire system is always subject to the overall electric neutrality condition:

$$-\int_{-\infty}^{\infty} \rho(x)dx = -e\sigma, \tag{A1}$$

where $\rho(x)$ is the total charge density of ions at x. This condition implies that at large distances from the surface the electric fields are vanishingly small, since the backbone charge is almost completely screened by surrounding ions.

The linearized Poisson-Boltzmann (PB) equation or the DH equation reads:

$$\frac{d^2\psi}{dx^2} = \kappa^2(x)\psi(x), \tag{A2}$$

where $\kappa(x)$ is the position-dependent inverse Debye length given by $\kappa(x) = 0$ for $-d < x < 0$ and $\kappa(x) \equiv \kappa = \sqrt{4\pi\ell_B\left[2n_1 + Zn_2(Z+1)\right]}$ otherwise (refer to Sec. 2.2.1). This equation can be solved with appropriate boundary conditions: at water-dielectric interfaces, the electric potential is continuous while the electric field is discontinuous. The jump in the normal component of the electric displacement field is $-4\pi e\sigma$. In addition, we assume that electric potential goes to zero as $x \to \pm\infty$, which results in zero total charge density at infinity. To summarize, the

boundary conditions read

$$x = 0 \quad : \quad \epsilon_> \partial_x \psi|_{0^+} - \epsilon_< \partial_x \psi|_{0^-} = -4\pi e\sigma \qquad (A3.1)$$

$$x = -d \quad : \quad \epsilon_< \partial_x \psi_d|_{-d+0^+} - \epsilon_> \partial_x \psi|_{-d-0^+} = 0 \qquad (A3.2)$$

$$x \to \pm\infty \quad : \quad \psi = 0. \qquad (A3.3)$$

Solving the DH equation subject to these conditions, we find electric potentials in three distinct regions:

$$\psi(x) = \begin{cases} \dfrac{-4\pi e\sigma}{\epsilon_> \kappa} \dfrac{\epsilon_< + \epsilon_> \kappa d}{2\epsilon_< + \epsilon_> \kappa d} e^{-\kappa x}, & x \geq 0 \qquad (A4.1) \\ \dfrac{-4\pi e\sigma}{2\epsilon_< + \epsilon_> \kappa d} \left(x + \dfrac{d}{2} \right) - \dfrac{2\pi e\sigma}{\epsilon_> \kappa}, & -d < x < 0 \qquad (A4.2) \\ \dfrac{-4\pi e\sigma}{\epsilon_> \kappa} \dfrac{\epsilon_<}{2\epsilon_< + \epsilon_> \kappa d} e^{\kappa(x+d)}, & x \leq -d \qquad (A4.3) \end{cases}$$

For similar calculations, see Refs. [11, 19] and references therein.

From these solutions we can easily infer the effect of dielectric discontinuities on charge distributions. At the DH level, total charge densities are proportional to electric potentials: $\rho = (\epsilon_>/4\pi)\kappa^2\psi$. As a result, one can simply write:

$$\rho(x = 0) \quad \propto \quad \frac{\epsilon_< + \epsilon_> \kappa d}{2\epsilon_< + \epsilon_> \kappa d}, \qquad (A5.1)$$

$$\rho(x = -d) \quad \propto \quad \frac{\epsilon_<}{2\epsilon_< + \epsilon_> \kappa d}. \qquad (A5.2)$$

It is instructive to take various limits: As $d \to 0$, the effect of dielectric discontinuities vanishes as expected. For $\epsilon_> \kappa d \gg \epsilon_<$, $\frac{\epsilon_< + \epsilon_> \kappa d}{2\epsilon_< + \epsilon_> \kappa d} \approx 1$. In this case, dielectric discontinuities become irrelevant. According to Eq. (*A*5.1), the charge density at the right side of the plate, (i.e., $x = 0$), increases as $\epsilon_< \to 0$. In other words, the dielectric jump there enhances the attraction of counterions to the surface. On the other hand, $\rho(x = -d)$ has the opposite behavior: it decreases as $\epsilon_<$ decreases. This tendency is consistent with the results in Fig. 2.3.

Now suppose both surfaces are charged with planar densities $\sigma_L \equiv \sigma(x = -d)$ and $\sigma_R \equiv \sigma(x = 0)$. To obtain electric potentials at the two surfaces, note that the

DH equation is linear. A linear combination of two DH solutions is a solution of the DH equation. If $\psi_{_R}(\sigma_{_L}=0,\sigma_{_R})$ ($\psi_{_R}(\sigma_{_L},\sigma_{_R}=0)$) is a potential at $x=0$ with $\sigma_{_L}=0$ ($\sigma_{_R}=0$), then the DH potential at the surface is $\psi_{_R}(\sigma_{_L},\sigma_{_R})=\psi_{_R}(\sigma_{_L}=0,\sigma_{_R})+\psi_{_R}(\sigma_{_L},\sigma_{_R}=0)$. Accordingly, the electric potential at the surface $x=0$ is

$$\psi_{_R}=-\frac{4\pi e\sigma_{_R}}{\epsilon_{_>}\kappa}\frac{(\epsilon_{_<}+\epsilon_{_>}\kappa d)}{(2\epsilon_{_<}+\epsilon_{_>}\kappa d)}-\frac{4\pi e\sigma_{_L}}{\epsilon_{_>}\kappa}\frac{\epsilon_{_<}}{(2\epsilon_{_<}+\epsilon_{_>}\kappa d)}. \qquad (A6)$$

Note that this satisfies the required boundary conditions at $x=-d$ and $x=0$. As a result, the chemical potential of counterions on the surface is

$$\frac{\mu_{_R}}{k_BT}=-\frac{4\pi\ell_B\sigma_{_R}}{\kappa}\frac{(\epsilon_{_<}+\epsilon_{_>}\kappa d)}{(2\epsilon_{_<}+\epsilon_{_>}\kappa d)}-\frac{4\pi\ell_B\sigma_{_L}}{\kappa}\frac{\epsilon_{_<}}{(2\epsilon_{_<}+\epsilon_{_>}\kappa d)}+\ln\left[\frac{\sigma_1(x=0)v_0}{\ell_c}\right]. \qquad (A7)$$

Similarly, we find the electric potential at the surface $x=-d$:

$$\psi_{_L}=-\frac{4\pi e\sigma_{_L}}{\epsilon_{_>}\kappa}\frac{(\epsilon_{_<}+\epsilon_{_>}\kappa d)}{(2\epsilon_{_<}+\epsilon_{_>}\kappa d)}-\frac{4\pi e\sigma_{_R}}{\epsilon_{_>}\kappa}\frac{\epsilon_{_<}}{(2\epsilon_{_<}+\epsilon_{_>}\kappa d)}. \qquad (A8)$$

This results in

$$\frac{\mu_{_L}}{k_BT}=-\frac{4\pi\ell_B\sigma_{_L}}{\kappa}\frac{(\epsilon_{_<}+\epsilon_{_>}\kappa d)}{(2\epsilon_{_<}+\epsilon_{_>}\kappa d)}-\frac{4\pi\ell_B\sigma_{_R}}{\kappa}\frac{\epsilon_{_<}}{(2\epsilon_{_<}+\epsilon_{_>}\kappa d)}+\ln\left[\frac{\sigma_1(x=-d)v_0}{\ell_c}\right]. \qquad (A9)$$

The results in Eqs. ($A7$) and ($A9$) are used to construct Fig. 2.3.

Appendix B

In this appendix, we derive the Debye-Hückel Green function $\phi(\mathbf{r}_\perp-\mathbf{r}'_\perp)$ introduced in Eq. (2.15) for a dielectric plate immersed in an ionic fluid. Note that similar problems have been studied in the literature [26, 27]. However, as they are, results presented in these references are not directly applicable to our problem for the reason explained in the text (see the relevant discussion below Eq. (2.16)). Here, we present the essential steps leading to $\phi(\mathbf{q})$ in Eq. (2.15). To this end, we use the Debye-Hückel (DH) approach to the system depicted in Fig. 2.1: a system with a non-uniform dielectric constant $\epsilon(\mathbf{r})$ and a position-dependent screening length $\kappa^{-1}(\mathbf{r})$. To appropriately incorporate dielectric discontinuities within the

DH approach, we first consider $\phi(\mathbf{r}, \mathbf{r}')$: the electric energy of a point charge e at $\mathbf{r}$ (the field point) due to another point charge e at $\mathbf{r}'$ (the source point) or simply the DH Green function. The DH equation for ϕ is then

$$\left[\nabla \cdot \epsilon(\mathbf{r})\nabla - \epsilon(\mathbf{r})\kappa^2(\mathbf{r})\right] \phi(\mathbf{r}, \mathbf{r}') = -4\pi e^2 \delta(\mathbf{r} - \mathbf{r}'). \qquad (B1)$$

Noting that ϕ has a translational invariance in the y-z plane, following Ref. [27], we express ϕ as a Fourier transform with respect to $y - y'$ and $z - z'$:

$$\phi(\mathbf{r}, \mathbf{r}') = \int \frac{d^2\mathbf{q}}{(2\pi)^2} e^{i\mathbf{q}\cdot(\mathbf{r}_\perp - \mathbf{r}'_\perp)} \phi(x, x', \mathbf{q}), \qquad (B2)$$

where $\mathbf{q}$ is the Fourier conjugate to $\mathbf{r}_\perp = (y, z)$.

If we use Eq. $(B2)$ in Eq. $(B1)$, we find

$$\left(\kappa^2 + q^2 - \frac{\partial^2}{\partial x^2}\right) \phi(x, x', \mathbf{q}) = \frac{4\pi e^2}{\epsilon_>} \delta(x - x'), \quad x \geq 0 \qquad (B3.1)$$

$$\left(q^2 - \frac{\partial^2}{\partial x^2}\right) \phi(x, x', \mathbf{q}) = \frac{4\pi e^2}{\epsilon_<} \delta(x - x'), \quad -d \leq x < 0 \qquad (B3.2)$$

$$\left(\kappa^2 + q^2 - \frac{\partial^2}{\partial x^2}\right) \phi(x, x', \mathbf{q}) = \frac{4\pi e^2}{\epsilon_>} \delta(x - x'), \quad x < -d \qquad (B3.3)$$

where κ^{-1} is Debye screening length defined in Sec. 2.2.1 and below Eq. $(A2)$. (Note that similar equations can be found in Ref. [27]. But we use different boundary conditions; see below). For the computation of $\phi(\mathbf{r}_\perp, \mathbf{r}'_\perp)$, it suffices to choose $\mathbf{r}' = (0, 0, 0)$ at the water-plate interface. In what follows, we drop x' from $\phi(x, x', \mathbf{q})$. Up to this point, the field point $\mathbf{r}$ can be anywhere; later it will be chosen to be at the plane $x = 0$ (see Eq. $(B.7)$).

The function $\phi(x, \mathbf{q})$ is continuous everywhere but its normal derivatives at $x = 0$ and $x = -d$ are discontinuous (as long as $\epsilon_> \neq \epsilon_<$):

$$\lim_{x \to -0} \epsilon_< \frac{\partial}{\partial x} \phi(x, \mathbf{q}) - \lim_{x \to +0} \epsilon_> \frac{\partial}{\partial x} \phi(x, \mathbf{q}) = 4\pi e^2, \qquad (B4.1)$$

$$\lim_{x \to -d-0} \epsilon_> \frac{\partial}{\partial x} \phi(x, \mathbf{q}) - \lim_{x \to -d+0} \epsilon_< \frac{\partial}{\partial x} \phi(x, \mathbf{q}) = 0. \qquad (B4.2)$$

As in the text, $\epsilon_<$ and $\epsilon_>$ are dielectric constants of the plate and water, respectively. The term on the right hand side of Eq. $(B1)$ is to reflect the source charge assumed to be located at $x = 0$.

With the boundary conditions in Eqs. ($B4$) and $\phi \to 0$ at $x = \pm\infty$, we find the solutions of Eqs. ($B3$) for $\mathbf{q} \neq 0$ [32]:

$$\beta\phi(x,\mathbf{q}) = \begin{cases} \dfrac{2\pi\ell_B}{\sqrt{\kappa^2+q^2}} e^{-x\sqrt{\kappa^2+q^2}} \dfrac{(1+\xi)\left(1-\xi e^{-2qd}\right)}{1-\xi^2 e^{-2qd}}, & x \geq 0 \qquad (B5.1) \\ \dfrac{2\pi\ell_B}{\eta q}\left(e^{xq} - \xi e^{-xq-2qd}\right)\dfrac{1-\xi}{1-\xi^2 e^{-2qd}}, & -d \leq x < 0 \quad (B5.2) \\ \dfrac{2\pi\ell_B}{\eta q} e^{(x+d)\sqrt{\kappa^2+q^2}} \dfrac{(1-\xi^2)e^{-qd}}{1-\xi^2 e^{-2qd}}, & x < -d \qquad (B5.3) \end{cases}$$

where $\beta = 1/k_BT$, $\ell_B = e^2/\epsilon_> k_BT$, $\eta = \epsilon_</\epsilon_>$, and ξ is defined in Eq. (2.16):

$$\xi = \frac{\epsilon_>\sqrt{\kappa^2+q^2} - \epsilon_< q}{\epsilon_>\sqrt{\kappa^2+q^2} + \epsilon_< q}. \qquad (B6)$$

For the $\mathbf{r} = (0, \mathbf{r}_\perp)$ (both the source and field points are in the same plane: $x = 0$), $\phi(0,\mathbf{q}) = \phi(\mathbf{q})$ is simplified as

$$\beta\phi(\mathbf{q}) = \frac{4\pi\ell_B}{\sqrt{\kappa^2+q^2}+\eta q}\left[1 + \xi\,(\xi-1)\,\frac{\exp(-2qd)}{1-\xi^2\exp(-2qd)}\right]. \qquad (B7)$$

This is identical to Eq. (2.15) in Sec. 2.3.2.

Chapter 3

Binding of Cationic Peptides onto a Negatively Charged Lipid Bilayer

3.1 Introduction

Antibacterial peptides such as Magainins, Defensins and Indolicidins are the main components of innate defense, which were discovered in animals as well as in plants [4, 33]. These peptides, typically made of 12-40 amino acid residues, target the cytoplasmic membranes of microorganisms. They have the ability to discriminate between host and microbial cells: they attach to the bacterial membranes, penetrate inside its bilayer and kill bacteria by permeablizing and/or disrupting their membrane while leaving the host cell intact. The major part of the membranes of living cells is their lipid bilayer, composed of self-assembled phospholipids, where proteins and other biomolecules are attached to it. The most sailent difference between bacterial and host cell membranes is the composition and topological arrangement of lipids in their bilayers [33]. The outer leaflet of host cell membranes is electrically neutral whereas the outmost leaflet of bacterial cell membranes contain large amount of negatively charged (acidic) phospholipids.

Antibacterial peptides typically have a number of positively charged amino acid

residues in their structure. As a result, they carry a net positive charge and would be attracted to oppositely charged membranes (e.g., bacterial membranes). This attraction has shown to play an important role in the activity and selectivity of antimicrobial peptides [4, 33–35]. Charged peptides are reported to have higher binding affinity for negatively charged biomembranes (e.g., bacterial membranes) than for electrically neutral membranes (e.g., the outer layer of eukaryotic cell membranes). In a number of experimental studies the binding affinity is shown to be stronger for more highly charged membranes [34,36,37]. These findings demonstrate the significance of the electrostatic interactions in peptide-lipid attraction, which will essentially create the selectivity of antimicrobial peptides.

Besides the electrostatic interactions between lipid bilayers and peptides, there are some other essential forces governing the dynamics and statics of such systems. Among others, the hydrophobic interactions turn out to play a crucial role [33, 38–40]. Hydrophobic force is responsible for penetration of peptides inside the lipid bilayer. Once adsorbed on the bilayer surface, a peptide can even penetrate inside the bilayer since some of the amino acid residues of the peptide are highly hydrophobic. These hydrophobic residues tend to insert the peptide inside the head-group area of the lipid bilayer, being in contact with lipids rather than water molecules. Penetration of the peptides inside the bilayer causes strain on the surface of the bilayer. As the density of the penetrated peptides reaches a threshold value, some transient pores start to form on the surface of the biomembrane, so as to relieve the unfavorable energy of membrane perturbation [33, 41]. Formation of these pores results in leakage of cell's content and/or translocation of peptides inside the cell, this finally gives rise to lysis of the cell's membrane [4, 33, 35].

This work is aimed at understanding the binding modes, thus surface activities, of antibacterial peptides. In particular, finding the density of bound peptides (peptides that are adsorbed on or penetrated inside the bilayer) as a function of the concentration of free peptides (those in bulk), electrical properties of the bilayer and the net charge of the peptides (We do not consider formation of pores on the bilayer). To this end, we introduce a three-state model in which peptides can be in one of the states of (*i*) free, (*ii*) surface adsorbed or (*iii*) penetrated inside head-group area of lipids, as depicted in Fig. 3.1. In our model, the details of which

will be discussed in the next section, peptide-peptide interactions on the surface are taken into account by assuming that peptides form a hexagonal lattice on the surface of the bilayer (Cf. Sec.3.2). The electrostatic energies are calculated taking into account the peptide-peptide interactions (on the surface) as well as the local changes in the composition of the lipids in the bilayer. The hydrophobic energy and entropic penalty for adsorption or penetration of peptides are added later regarding the fact that these energies are independant of electrostatic interactions between pepetides and salt ion, i.e., they are not influenced by peptide-peptide interactions on the surface of the bilayer.

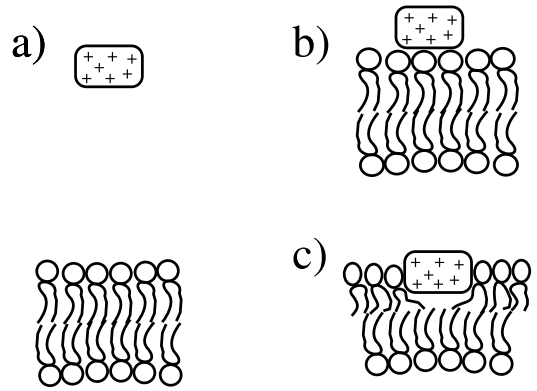

Figure 3.1: Schematic representation of peptides in three different states: (a) A free peptide in bulk, (b) Surface adsorbed peptide and (c) a peptide inserted inside the head-group region.

3.2 Theoretical Model And Wigner-Seitz Cell Approximation

The lipid bilayer is assumed to be a two-dimensional binary fluid mixture of zwitterionic (electrically neutral) and monovalent acidic (negatively charged) lipids which are ideally mixed in the absence of charged macromolecules around the bilayer. The charge density of the bilayer is determined by the fraction of charged lipids, i.e, number of charged lipids/total number of lipids, $\overline{\alpha}$ ($0 \leq \overline{\alpha} \leq 1$), and the area occupied

by the head-group of each lipid, a. Since the charge of acidic lipids is equal to the electronic charge, $-e$, the surface charge density of the bilayer can be written as $\sigma = -e\overline{\alpha}/a$. For simplicity all lipids are assumed to have the same headgroup area and membrane proteins are not included.

Molecular details of peptides are largely ignored. They are modeled as uniformly charged disks with a negligible thickness, radius R_p and, electric charge of Q_p. These disks thus have a constant surface charge density of $Q_p/\pi R_p^2$.

The bilayer is immersed in an electrolyte with dielectric constant of $\epsilon = 80$ containing negative and positive monovalent ions (e.g., Na^+ and Cl^-) with densities of $[Na^+] = [Cl^-] = n_0$ at large distances from the bilayer and any other macromolecule, where the electric potential is effectively zero. In the presence of these ions, the electrostatic interactions are screened. The screening length (or Debye length), κ^{-1}, is given by $\kappa^2 = 8\pi n_0 e^2/\epsilon k_B T$ where e is the electronic charge and $k_B T$ is the thermal energy. In addition to the salt ions, we also consider some peptides in the solution (charged disks in our model). Carrying an electric charge, peptides can interact with each other, with ions or with the bilayer via electrostatic forces. The concentration of peptides at bulk, C_f, is assumed to be low enough so that peptide-peptide interactions can be ignored in this region (peptides in this region are also referred to as "free peptides"). Due to the screening effect of the salt ions there would be no significant interaction between the bilayer and free peptides. In the close vicinity of the lipid bilayer, however, the electrostatic attraction between the peptide and bilayer can be important. In this region, the peptide can bind to the bilayer electrically. At the same time, this binding can influence the distribution of charged and neutral lipids in the bilayer. When there is no highly charged macromolecule on the surface of the bilayer, neutral and charged lipids are ideally mixed, ı.e., the local fraction charged lipids, α, is constant over the bilayer's surface. Upon adsorption of a positively charged macromolecule on the bilayer, lipids are redistributed (demixed) so that the density of negatively charged lipids increases near the positively charged macromolecule. This change of the local composition of the lipids, which is not entropically favorable, can reduce the free energy of the system by lowering the electrostatic energy as discussed in a number of experimental works [42, 43].

On the bilayer, peptides can be in either "surface adsorbed" or "penetrated" state. Surface adsorbed peptides are those that are attached to the surface of the bilayer (Fig. 3.1). This state is driven by the electrostatic attraction between peptides and charged lipid headgroups. Beside this state, some of the peptides are penetrated inside the head-group region of the lipids. In this case, the peptide pushes the head-groups of lipids aside forcing a gap to form inside the bilayer. It is, however, known that the fatty tails of the lipids fill any gap and prevent gap formation by decreasing the local thickness of the bilayer. Due to the elasticity of the bilayer, there ia a mechanical energy cost associated with adsorption or penetration of the peptides, given by $\frac{1}{2}K_a\Delta A^2/A$, where K_a is the stretching modulus of one leaflet of the bilayer, i.e., one monolayer, A is the area of the bilayer and ΔA is the area increment caused by penetration and adsorption of peptides (in other words, difference between the area of the bilayer, A, and its equilibrium).

Peptide densities in different states can be calculated by balancing their chemical potentails. Since the concentration of peptides at bulk (free peptides) is low, peptide-peptide interactions can be ignored and the chemical potential of the peptides at bulk solution is mainly from the configurational entropy of the mixing and thus given by $\mu_{free} = k_BT\ln(C_f v_p)$, where k_B is the Boltzmann constant, T temperature, and v_p is the volume of a peptide. Note that here and in what follows, electical free energies of peptides are calculated with respect to the charging energy of one single peptide in bulk solution (peptide-peptide interactions are ignored). Computation of the chemical potentials of surface adsorbed and penetrated peptides is complicated by peptide-peptide interactions on the bilayer. The density of the peptides in these states, as evidenced in experimental works [37–39], are typically high enough that peptide-peptide repulsion needs to be taken into account. To this end, we present a hexagonal lattice model for peptides on the bilayer. In this model, each peptide on the surface is surrounded by six other peptides being at equal radial distance of $2R$. Based on this assumption, peptides on the surface, regardless of the state they are in, define a two-dimensional Wigner-Seitz (WS) cell with radius R as depicted in Fig. 3.2. With this model, chemical potentials of peptides on the bilayer can be obtained from the free energy of one WS cell. In this section, we find the free energy of one WS cell based on minimization of the

functional form of the free energy. The next section will be devoted to computation of chemical potentials of peptides on the surface in different states.

The Wigner-Seitz cell scheme as an approximation for the arrangement of charged particles on a charged surface has been used in different works before. Owicki and McConnell used this method for protein-lipid and protein-protein interactions on the bilayer membrane [44]. Nguyen and colleagues used this lattice model for the adsorption of ions on a uniformly charged surface [45]. This method was also used for charged spherical particles (model of charged protein) interacting with each other and a lipid bilayer at a constant distance form the surface [46]. The drawback of the WS cell method for such systems is that it supresses the lateral fluctuations of the adsorbates. This problem can be, however, remedied to some extent by adding an entropic part to the free energy of the system which treats the adsorbates as particles that can change their positions on the surface, i.e., an entropic term that is proportional to the logarithm of the density of adsorbates. In general, the WS lattice model is more accurate in two limiting cases: when the density of adsorbate is sufficiently low on the surface and when the density of adsorbates is high enough. In the former, there is no interaction among the adsorbates on the surface and thus the system reduces to one adsorbate on the surface. In this case it is not important how we assume the arrangement and geometrical distribution of the adsorbate. In the later, the repulsion force between adsorbates (in our system peptides) makes them form a hexagonal lattice on the surface. In the intermediate level, lateral fluctuations of adsorbate can reduce the accuracy of the model.

The Wigner-Seitz (WS) cell in our model consists of one charged disk (model of a peptide) which is on the bilayer of low dielectric constant (≈ 2). This disk can be adsorbed on the surface or penetrated inside the head-group area. Since we ignore the thickness of the disk the only difference between these two states comes from the distribution of the lipids on the bilayer: when the peptide is penetrated, lipid head-groups cannot move to the area occupied by the peptide; when the peptide is adsorbed on the surface, however, lipids can migrate to this region as depicted in Fig. 3.3. The functional form of the free energy that we use for a WS cell arises from the entropy of the mobile ions and lipids, as well as the electrostatic energy

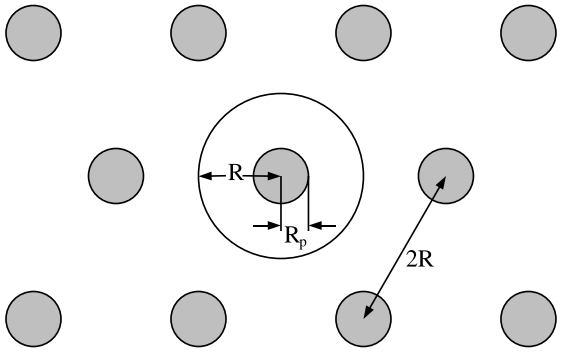

Figure 3.2: Schematic picture of peptides forming a hexagonal lattice on the surface (top view).

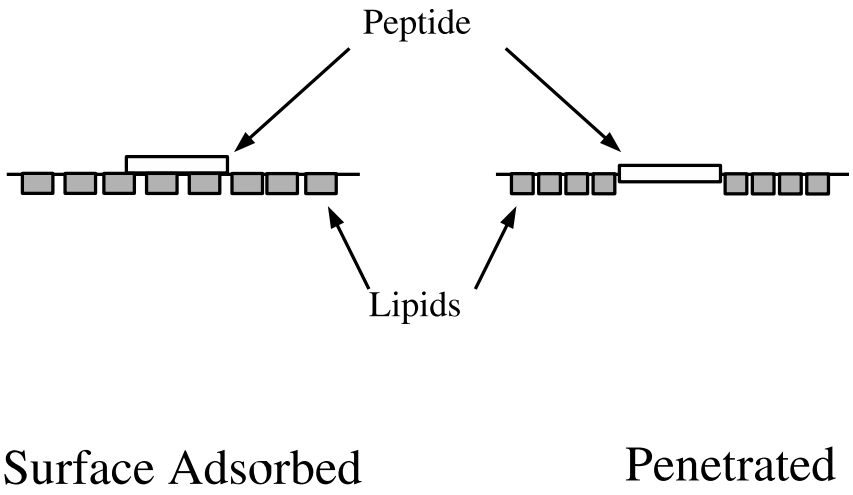

Figure 3.3: Schematic picture of adsorption and penetration of peptides (side view).

of the system:

$$\begin{aligned}\frac{\mathcal{F}}{k_BT} &= \frac{1}{2}\frac{\epsilon}{k_BT}\int_V (\nabla\Phi)^2 dv \\ &+ \int_V \left[n_+ \ln\frac{n_+}{n_0} + n_- \ln\frac{n_-}{n_0} - (n_+ + n_- - 2n_0)\right] dv \\ &+ \frac{1}{a}\int_a \left[\alpha \ln\frac{\alpha}{\overline{\alpha}} + (1-\alpha)\ln\frac{1-\alpha}{1-\overline{\alpha}}\right] ds \\ &+ \lambda\frac{1}{a}\int_a (\alpha - \overline{\alpha}) ds, \end{aligned} \tag{3.1}$$

where $\Phi = \Phi(r, z)$ is the electrostatic potential, ϵ the dielectric constant of the solvent, $n_+ = n_+(r, z)$ and $n_- = n_-(r, z)$ densities of positive and negative monovalent ions, respectively, $\alpha = \alpha(r)$ and $\overline{\alpha}$ are the local and average fraction of the charged lipids in the bilayer, and a is the area of each head-group (assumed to be the same for charged and neutral lipids).

The first term in Eq. 3.1 is the electrostatic energy of the system where the integral runs over the whole volume of the WS cell. The second term accounts for the change in the entropy of salt ions. Near charged molecules, density of positive (negative) mobile ions, n_+ (n_-), are altered due to electrostatic interactions. Far away from any charge molecule we have $n_+ = n_- = n_0$ and thus there would be no change in entropy. The third term takes the entropic penalty of the lipid demixing into account and the integral is over the bilayer within the WS cell. Here we should note that when the peptide is penetrated, the head-group area of the lipids, a, reduces so that the peptide can be accommodated in the head-group region. This process affects the third term in the free energy. The last term is added to impose the charge conservation condition in the WS cell. λ is the Lagrange parameter and is determined by the charge conservation condition.

The dielectric constant of the bilayer is assumed to be much smaller than that of the electrolyte. The thickness of lipid bilayer is about 40Å and the Debye length of the electrolyte is about 10−100Å. Given this thickness, the dielectric constant of the bilayer and the debye screening length, there would be no electrostatic interaction between peptides and ions in one side of the bilayer with other charged particles on the other side of the bilayer [47]. In this case, the bilayer acts similar to an

infinitely thick insulator and we can safely ignore the free energy associated with the mobile ions and lipids on the other side of the bilayer.

The minimization of the free energy, $\mathcal{F}$, with respect to the densities of the mobile ions (n_+ and n_-) and the local fraction of charged lipids (α) gives the non-linear Poisson-Boltzmann equation for the electric potential in the aqueus phase,

$$\nabla^2\Phi = \frac{k_BT\kappa^2}{e}\sinh\left(\frac{e\Phi}{k_BT}\right), \tag{3.2}$$

where κ is the inverse debye length and e is the electronic charge. The relation for the local fraction of charged lipids is obtained as

$$\alpha = \frac{\exp\left(\frac{e\Phi}{k_BT} - \lambda\right)}{\frac{1-\overline{\alpha}}{\overline{\alpha}} + \exp\left(\frac{e\Phi}{k_BT} - \lambda\right)}. \tag{3.3}$$

In order to find the electrostatic potential in the WS cell we need to solve Eq. 3.2 subject to the boundary conditions. The boundary conditions reflect the properties of Φ at the WS cell as well as the surface charge density of the bilayer and the potential at infinity. On the WS cell boundary we impose

$$\left.\frac{\partial\Phi}{\partial r}\right|_{r=R_p} = 0, \tag{3.4}$$

where r is the radial distance form the center of the WS cell and R_p is the radius of the cell. This condition forces the electric field to vanish on the boundary of the cell. On the interface between electrolyte and the bilayer, the normal derivative of the electric field is determined by the surface charge density $\sigma = -e\alpha/a$. Since the dielectric constant of the bilayer is much less than that of the electrolyte we assume that electric field cannot penetrate inside the lipid area. Thus we have

$$\left.\frac{\partial\Phi}{\partial z}\right|_{z=0} = \begin{cases} -\dfrac{e\alpha}{\epsilon a}, & r > R_p \\ -\dfrac{e\alpha}{\epsilon a} + \dfrac{Q_p}{\pi R_p^2}, & r \le R_p, \end{cases} \tag{3.5}$$

where z denotes the distance from the bilayer's surface and ϵ is the dielectric constant of the electrolyte. For penetrated peptides, a changes to a new value and the first term for $r \leq R_p$ in Eq. 3.5 is turned off. The density profile of the lipids on the surface should be determined by the combination of the Eqs. 3.3 and 3.5. These equations are solved *self-consistently* with Eq. 3.2.

To solve the problem numerically, we used the *finite element* numerical method. Due to the cylindrical symmetry of the WS cell it suffices to take a two dimensional grid point mesh to represent the potentials in our three dimensional space. Density of grids in r direction (distance from the center of the cylindrical cell) is 5 grid points per Å and is constant for different values of z (distance from the bilayer). In the z direction, a total number of 70 grids are chosen, distance between these grid points increases exponentially as a function of z. The meshing scheme thus provides more dense grids near the bilayer's surface and the density of grids decreases exponentially as z increases. The electric potential (Φ), the density of salt ions (n_+ and n_-) and composition of the lipids on the bilayer (α) are found simultaneously. The free energy, $\mathcal{F}$, is then calculated according to Eq. 3.1.

The adsorption or penetration free energy of one WS cell containing a peptide is given by

$$\begin{aligned} \mathcal{F}_a &= \mathcal{F} - \mathcal{F}_0 \\ \mathcal{F}_p &= \mathcal{F} - \mathcal{F}_0 + \mathcal{E}_p, \end{aligned} \tag{3.6}$$

where $\mathcal{F}$ is obtained from the functional form in Eq. 3.1 (its value is different for surface adsorbed and penetrated peptides), $\mathcal{F}_0$ is the sum of charging free energy of one single peptide at bulk (the peptide is fixed in space and peptide-peptide interactions are ignored) and the free energy of an unperturbed bilayer in the solution with the surface charge density of $\sigma = -e\overline{\alpha}/a$ and area of πR^2. The last term for $\mathcal{F}_p$ in Eq. 3.6 is added to account for other effects including hydrophobic energy. This term is not influenced by peptide-peptide interactions and thus are not dependent on WS cell radius. In the next section, we also take the mechanical energy of the bilayer into account which does not depend on electrostatic interactions, yet is a function of the peptides density. Using these free energies, $\mathcal{F}_a$ and $\mathcal{F}_p$, we calculate chemical potentials of the peptides in different states.

3.3 Binding Isotherm

Densities of surface adsorbed and penetrated peptides can be found by balancing chemical potentials of peptides in different states. In this section we calculate chemical potentials of the peptides. To this end, we first find the free energy of the bilayer and peptide system (per unit area) based on the results of the previous section. Let σ_a and σ_p be the densities of the peptides in surface adsorbed and penetrates states, respectively. Consider a bilayer with the area of A whose outer layer area, including peptides, remains constant. The free energy of the combination of the lipid bilayer and peptides (surface adsorbed and penetrated peptides) per unit area can be written as

$$F = \sigma_a \mathcal{F}_a + \sigma_p \mathcal{F}_p + \frac{1}{2} K_a \left(\frac{\Delta A}{A} \right)^2 + k_B T \left[\sigma_a \ln(\sigma_a A_p) - \sigma_a + \sigma_p \ln(\sigma_p A_p) - \sigma_p \right] \quad (3.7)$$

The first two terms in Eq. 3.7 correspond to the electrostatic energy of the peptides, the mixing entropy of the lipids and the entropy of mobile ions in the solution according to our definition of $\mathcal{F}$ in Eq. 3.1, $\mathcal{F}_a$ and $\mathcal{F}_p$ in Eq. 3.6. The third term accounts for the mechanical energy cost of the peptide binding. K_a is the stretching modulus of the lipid layer (we assume that it is not altered by penetration and adsorption of peptides), (ΔA) is the extension or compression of the bilayer from its equilibrium state and A is the equlibrium area of the bilayer in absence of the peptides. The last two terms account for the mixing entropy of the peptides. Note that the peptide-peptide repulsions on the surface are implicitly taken into account in $\mathcal{F}_a$ and $\mathcal{F}_p$ through the Wigner-Seitz cell radius, R. The dependence of $\mathcal{F}_a$ and $\mathcal{F}_p$ on the densities, i.e., σ_a and σ_p, through R, determines the dependence of F on the densities of the peptides and on the peptide-peptide repulsions. Nevertheless, the last two terms, entropic terms, also depend on R since σ_a and σ_p can be related to R.

ΔA is mainly determined by two opposing factors: compression of the lipids, caused by penetration of the peptides; and lateral pressure on the charged lipids, due to adsorption or penetration of peptides, i.e., attraction of the lipids to the peptide which shrinks the head-group of lipids and thus decreases the equilibrium

area of the bilayer. In terms of a WS cell, the area of the cell (πR^2) and the number of lipids in the cell remains constant after adsorption of a peptide. The equilibrium area, however, decreases by peptide adsorption. Therefore, adsorption of a peptide results in stretching of the surface from its equilibrium state. When a peptide penetrates inside the head-group region, the area of the WS cell occupied by lipids, thus the head-group area of each lipid, decreases. In this case, compression of the lipids is partially because of the lateral electric pressure on the surface, and partially because of the repulsion of the lipids from the hard disk peptide (i.e, lipids can't move to the area occupied by the peptide). In the appendix of this chapter we present our calculation scheme for the computation of such area changes. ΔA_p^{eq} and ΔA_a^{eq} denote the difference between the area of a WS cell, πR^2, and the equilibrium area that the surface (inside the WS cell) could reach if it was not connected to the rest of the bilayer for a penetrated or surface adsorbed peptide, respectively. According to the density of the peptides on the surface, ΔA can be written as

$$\frac{\Delta A}{A} = -\sigma_p(A_p + \Delta A_p^{eq}) - \sigma_a \Delta A_a^{eq} \tag{3.8}$$

ΔA_p^{eq} and ΔA_a^{eq} are negative showing that equilibrium area is decreased by the lateral tension imposed by peptide on the surface.

Taking the derivative of the Eq. 3.7 with respect to the density of the peptides in each state gives the chemical potential of the peptides:

$$\begin{aligned} \mu_i &= \frac{\partial F}{\partial \sigma_i} \\ &= \mathcal{F}_i + \sigma_a \frac{\partial \mathcal{F}_a}{\partial \sigma_i} + \sigma_p \frac{\partial \mathcal{F}_p}{\partial \sigma_i} + \frac{1}{2} K_a \frac{\partial}{\partial \sigma_i} \left(\frac{\Delta A}{A} \right)^2 + k_B T \ln(\sigma_i A_p), \end{aligned} \tag{3.9}$$

where i denotes the state of the peptide, i.e., $i = a$ or p. Since in our calculations $\mathcal{F}_p$ and $\mathcal{F}_a$ are found as a function of WS radius, R, we need to rewrite Eq. 3.9 in terms of R. Instead of using σ_a and σ_p, we can use R and f as two independent variables defined as

$$R = \left[2\sqrt{3}(\sigma_a + \sigma_p)\right]^{-1/2},$$
$$f = \frac{\sigma_p}{\sigma_a + \sigma_p}. \tag{3.10}$$

The first equation in Eq. 3.10 reflects the fact that peptides form a hexagonal lattice on the surface. One peptide occupies the area equal to $2\sqrt{3}R^2$ on the surface. The density of all peptides peptides $(\sigma_a + \sigma_p)$ can be thus related to the radius of the WS cell. The second equation defines the fraction of penetrated peptides on the surface. Using Eq. 3.10 and assuming that $\frac{\partial \sigma_a}{\partial \sigma_p} = \frac{\partial \sigma_p}{\partial \sigma_a} = 0$, Eq. 3.9 can be rewritten in terms of R and f as

$$\mu_i(R, f) = \mathcal{F}_i - \frac{1}{2}R\left[(1-f)\frac{\partial \mathcal{F}_a}{\partial R} + f\frac{\partial \mathcal{F}_p}{\partial R}\right] \tag{3.11}$$
$$+\frac{1}{2}K_a\frac{\partial}{\partial \sigma_i}\left(\frac{\Delta A}{A}\right)^2 + k_B T \ln(\sigma_i A_p).$$

Here again, i denotes the state of the peptide which can be either a or p. In writing Eq. 3.12 we used the fact that in our formalism $\mathcal{F}_a$ and $\mathcal{F}_p$ are functions of R and do not depend on the fraction of penetrated peptides, f, $(\frac{\partial \mathcal{F}_p}{\partial f} = \frac{\partial \mathcal{F}_a}{\partial f} = 0)$. We should note that this is an approximation which is a result of Wigner-Seitz cell calculation scheme. In equlibrium condition, chemical potentials of peptides are balanced. We thus have

$$\mu_a(R, f) = \mu_{free}$$
$$\mu_p(R, f) = \mu_{free} \tag{3.12}$$

Solving these equations for R and f, we can obtain densities of surface adsorbed and penetrated peptides using $\sigma_p = f/2\sqrt{3}R^2$ and $\sigma_a = (1-f)/2\sqrt{3}R^2$.

3.4 Results and Discussions

3.4.1 Redistribution of Lipid Charges Upon Peptide Binding

As the peptides reach the surface of the lipid bilayer, the electrostatic attraction between charged lipids and peptides alters the distribution of the lipids. The local fraction of negatively charged lipids, α, increases near the peptide and decreases at larger distances from the peptides. In our model we assumed that the head-group area of lipids, a, is the same for the charged and neutral lipids in a Wigner-Seitz cell; as a result, the density of lipids is uniform in the WS cell. However, the fraction of charged lipids is position-dependetnt. When a peptide penetrates inside the head-groups, lipids cannot migrate to the region occupied by the peptide. They are thus accomodated in the rest of the WS cell area while their head-groups are shrinked.

As depicted in Fig. 3.4 higher fractions of charged lipids are observed near the peptide; α decays as the distance from the peptide increases. Due to the charge conservation condition in the WS cell (in other words, conservation of lipids) we have $\int_{r=0}^{R} 2\alpha\pi r dr = \overline{\alpha}\pi R^2$. As can be seen from Fig. 3.4, the lowest fraction of charged lipids, $\alpha(r = R)$, varies with radius of WS cell, R. When R increases, $\alpha(r = R)$ gets closer to the average fraction, $\overline{\alpha}$. For $R \to \infty$ we have $\alpha(r = R) = \overline{\alpha}$. This case corresponds to the adsorption or penetration of one single peptide on the surface of a lipid bilayer. In this limit, the Wigner-Seitz cell approximation does not play any role since the system is not influenced by peptide-peptide interactions. Here we note that the lagrange factor λ is found by the condition of charge conservation in the WS cell according to Eq. 3.3; the last term in Eq. 3.1 will vanish after imposing this condition.

3.4.2 Free energy of a Wigner-Seitz cell

In Sec.II we introduced the Wigner-Seitz cell approximation scheme and presented a method to calculate the free energy of a WS cell. In this section, we present

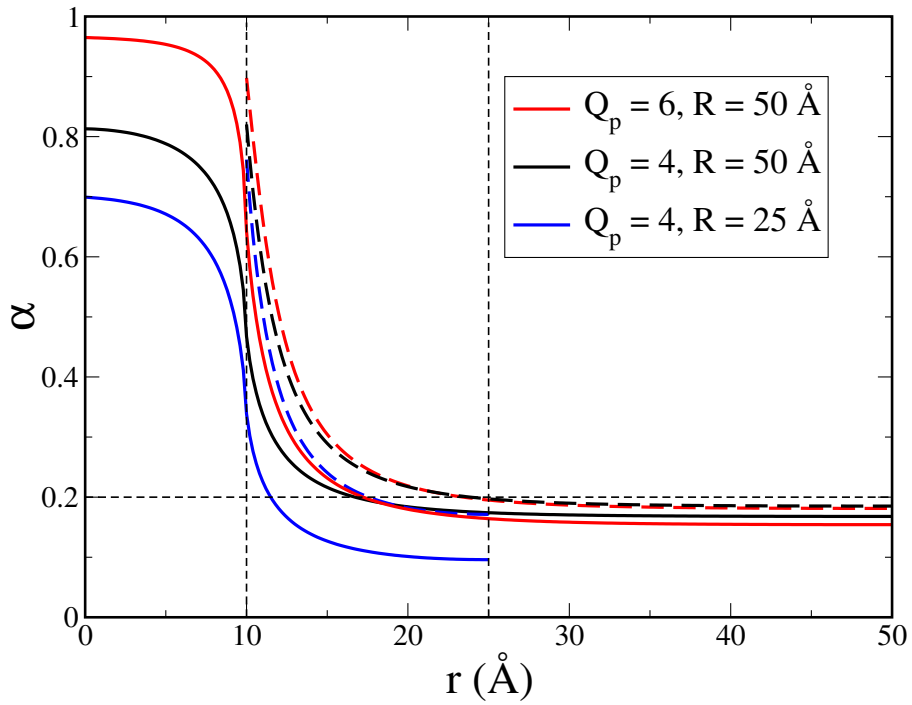

Figure 3.4: Local fraction of charged lipids as a function of the radial distance from the center of and adsorbed (solid lines) and a penetrted peptide (dashed lines) for two different radii of the Wigner-Seitz cell, $R = 25$ and $R = 50$. Here $\overline{\alpha} = 0.2$ and $Q_p = 4$ and 6.

our results for $\Delta\mathcal{F} = \mathcal{F} - \mathcal{F}_0$ where $\mathcal{F}$ is the free energy of a WS cell defined in Eq. 3.1 and $\mathcal{F}_0$ is the charging free energy of one fixed single peptide in bulk and an unperturbed membrane (for more details refer to Sec. 3.2 below Eq. 3.6). $\Delta\mathcal{F}$ is the free energy of a WS cell excluding the mechanical part. $\Delta\mathcal{F}$ explicitely depends on charge properties of peptide and lipids as well as the solution. Thus, a detailed analysis of $\Delta\mathcal{F}$ gives us a physical insight on the effects of the electrical properties of the system on penetration and adsorption of peptides.

$\Delta\mathcal{F}$ is mainly affected by three major factors: peptide-lipid attractions, peptide-peptide repulsions on the surface and interaction of peptides with their *image* charges. Since the dielectric constant of the lipid bilayer is much less than that of water, the dielectric discontinuity can be important near the interface. In electrostatic systems with dielectric discontinuities, image charges can be introduced to take these discontinuities into account. When image charges are included in the system, the dielectric constant of the system should be assumed constant. In our calculation scheme, described in Sec.3.2, we explicitly considered low dielectric constant for lipids (Eq. 3.5). Therefore, there was no need to include this effect through image charges in the system. Later in this section, however, we will use image charge descriptions to explain our results from a more physical point of view.

Fig. 3.5 shows the results for $\Delta\mathcal{F}$ as a function of WS cell radius, R for different peptides charge, $Q_p = 6$ and 8, and different fractions of charged lipids, $\overline{\alpha} = 0.15$ and 0.30. Increasing the fraction of charged lipids, $\overline{\alpha}$, (reminiscent of increasing negative charge density of lipid bilayer) results in lower (ı.e., more negative) $\Delta\mathcal{F}$. This arises from a stronger attraction between a peptide and the lipid bilayer. As can be seen in Fig. 3.5 increasing $\overline{\alpha}$ has the same effect on penetrated and surface adsorbed peptides namely in both cases, peptides have a higher binding affinity for highly charged surfaces than for surfaces with lower charge densities. This is indeed consistent with results of experimental works [36].

The effect of the peptide-peptide repulsions, as mentioned before, are taken into account through the radius of WS cell in our model. A smaller radius of the WS cell corresponds to a closer distance and stronger repulsion between peptides resulting in larger values for $\Delta\mathcal{F}$ as evidenced in Fig. 3.5. In the limit $R \to 0$, larger free energy is expected for highly charged peptides than peptides with lower electric charge (of

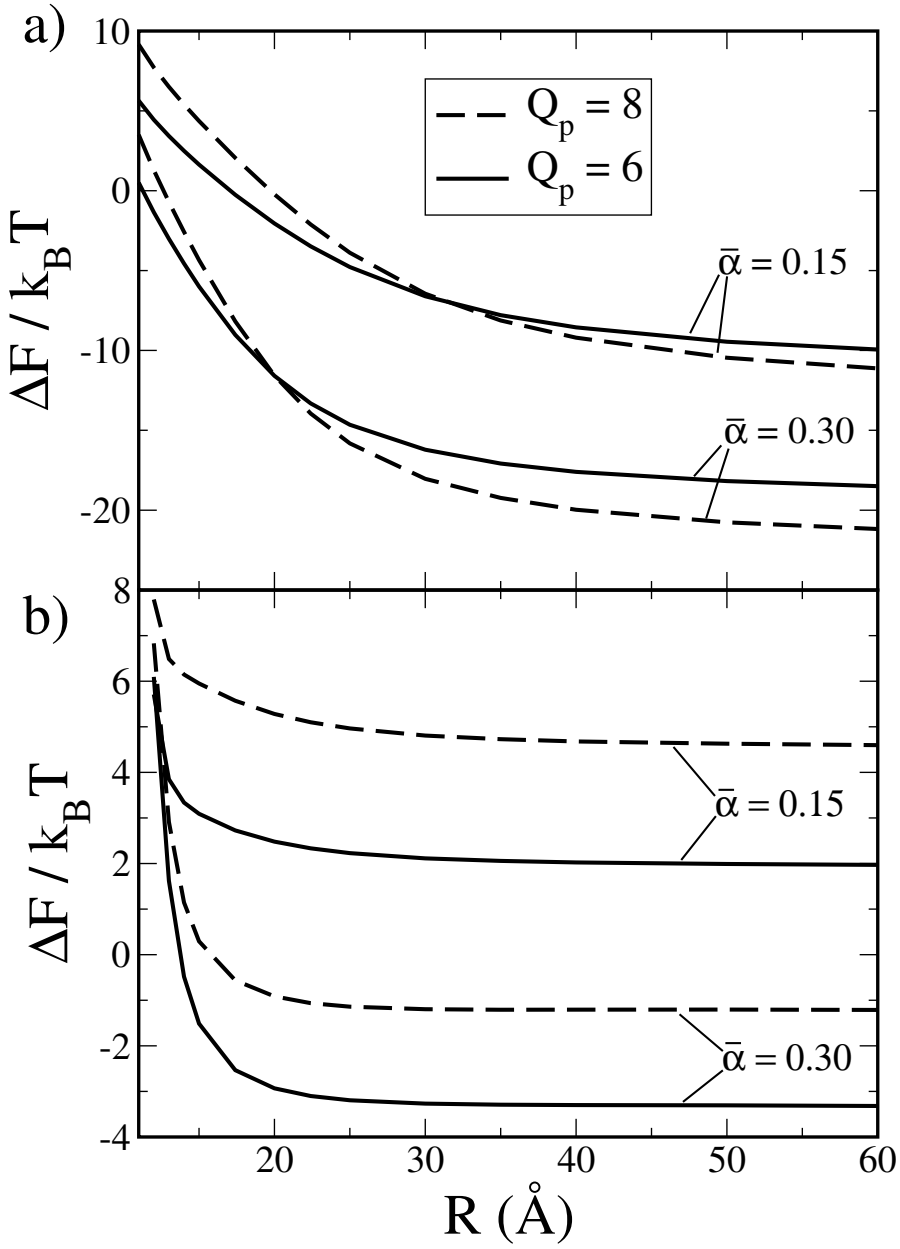

Figure 3.5: Free energy of a WS cell (excluding the mechanical energy), $\Delta\mathcal{F}$, as a function of the radius of Wigner-Seitz cell radius for surface adsorbed (a) and penetrated (b) peptides. Average fraction of charged lipids are chosen as $\overline{\alpha} = 0.15$ and 0.30. Curves are plotted for two different peptide charge: $Q_p = 8$ (dashed line) and $Q_p = 6$ (solid line).

course if other parameters remain constant). This shows that accumulation of highly charged peptides can be hindered by peptide-peptide repulsions. In the limit $R \to \infty$, the peptide-peptide repulsion is minimal as the system reduces to a single peptide bound to the bilayer. In this limit, where the peptide-lipid bilayer attraction and peptide interactions with image charges are dominant, effects of changing the peptide charge on the free energy depend on the fraction of charged lipids, $\overline{\alpha}$. Fig. 3.6 shows $\Delta\mathcal{F}(R \to \infty)$, i.e., $\Delta\mathcal{F}$ in the limit $R \to \infty$ in which peptide-peptide repulsions are "turned off", as a function of the peptide's charge, Q_p, with different fractions of charged peptides, $\overline{\alpha}$. For penetrated peptides, $\Delta\mathcal{F}$ monotonically increases as Q_p increases. For surface adsorbed peptides, the curve with lowest $\overline{\alpha}$ $(= 0.05)$ shows that $\Delta\mathcal{F}$ increases with increasing Q_p. For larger values of $\overline{\alpha}$, however, a higher charge on peptides can lower the free energy of the WS cell. Effects of peptide charges can be explained in terms of image charges. Since the dielectric constant of lipids is much less than that of water, a peptide's image charge has the same charge as the peptide, which results in repulsion of the peptide from the surface of the lipid bilayer. For penetrated peptides, in the limit $R \to \infty$, this effect is dominant because there is no charged lipid between the peptide and the bilayer. Thus, penetration of highly charged peptides inside a bilayer with low dielectric constant can be hindered because of the high free energy cost associated with peptide-image charge interactions. There is, however, a different scenario when the peptide is adsorbed on the surface and is not penetrated inside the bilayer. In this case, since the charged lipids can move under the peptide, i.e., the area that the peptide is adsorbed on, increasing the peptide charge gives rise to a higher number of negatively charged lipids in the intimate vicinity of the peptides. These lipids can then neutralize peptide charges, decrease the repulsion between the peptide and its image charge and at the same time decrease the electrostatic energy associated with peptide-lipids attraction. This process can lower the energy of the system unless the mean fraction of charged lipids, $\overline{\alpha}$, is too low. If $\overline{\alpha}$ is too low, then there would be a high entropic penalty for the lipids to efficiently neutralize peptides charge. In this case, highly charged peptides have a lower affinity for the lipid bilayer's surface than peptides with lower charges.

We have also calculated $\Delta\mathcal{F}(R \to \infty)$ for penetrated peptides in the case that

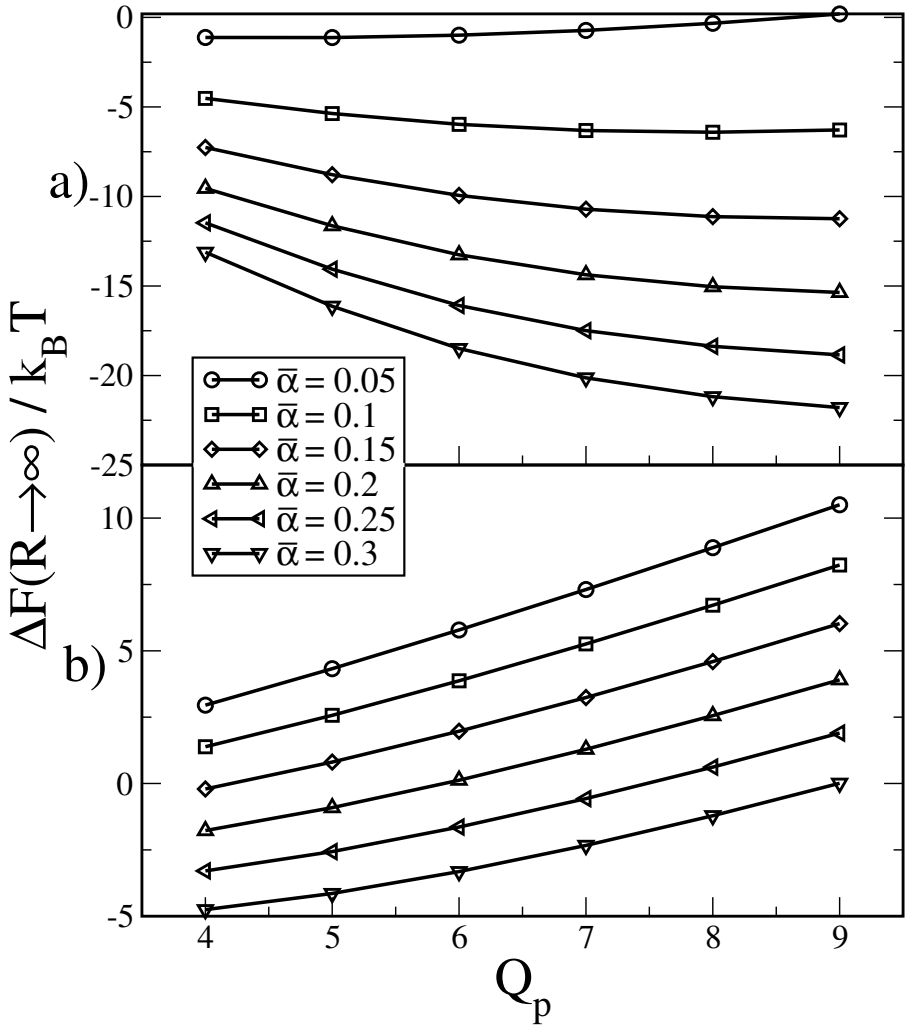

Figure 3.6: Free energy of an infinitly large WS cell (excluding the mechanical energy), $\Delta\mathcal{F}(R \to \infty)$, as a function of the peptide charge, Q_p for surface adsorbed (upper figure) and penetrated peptides (lower figure). These curves correspond to different values of $\overline{\alpha}$. For large values of $\overline{\alpha}$, $\Delta\mathcal{F}(R \to \infty)$ tends to decrease as Q_p increases.

there is no dielectric discontinuity and thus no image charges. Results are plotted in Fig. 3.7. Since there is no image charge-peptide repulsion, increasing peptides charge always lowers the free energy of binding, unlike the Fig. 3.6 where the interactions of peptide with the image charges increased $\Delta\mathcal{F}(R \to \infty)$.

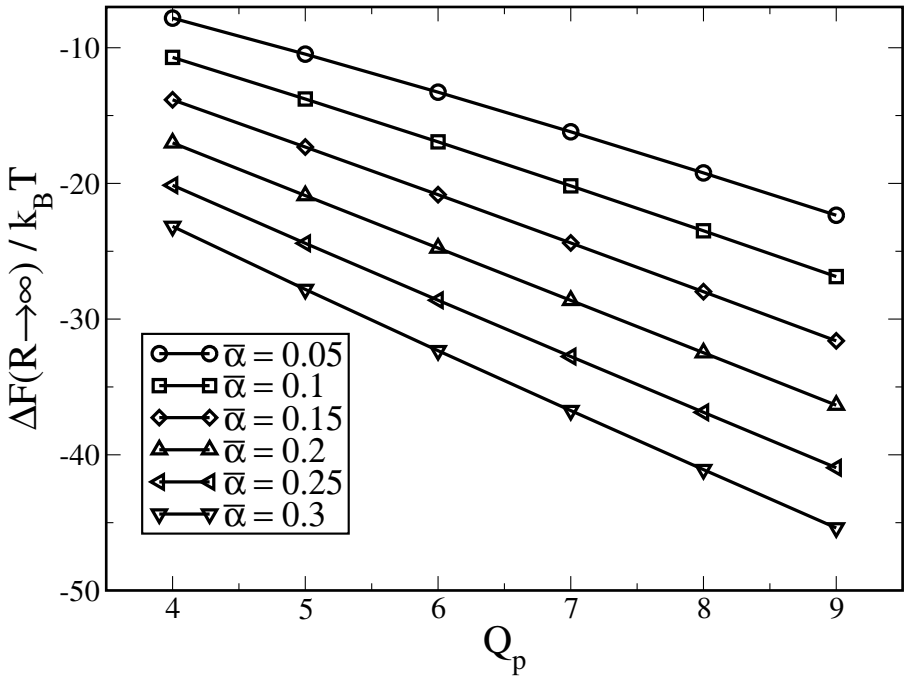

Figure 3.7: Free energy of an infinitly large WS cell (excluding the mechanical energy), $\Delta\mathcal{F}(R \to \infty)$, as a function of peptide charge, Q_p, when there is no dielectric discontinuity in the system. These curves correspond to different values of $\overline{\alpha}$. $\Delta\mathcal{F}(R \to \infty)$ decreases with increasing peptide charge.

In the next section, we use $\mathcal{F}_a$ and $\mathcal{F}_p$ combined with other effective energies, e.g., entropy of the peptide distrinution on the surface and mechanical energy, to find density of penetrated and surface adsorbed peptides as a function of the bulk concentration of the peptides.

3.4.3 Adsorption and penetration

Highly Hydrophobic peptides with a low net charge

Peptides with highly hydrophobic residues and low net charge have a great tendency for penetration inside the bilayer. For these peptides, fraction of penetrated peptides is close to one ($f \approx 1$) due to the lower free energy associated with penetration in comparision with the free energy of surface adsorbed state. Low peptide charge results in lower peptide-image charge repulsion, encouraging penetration. Fig. 3.8 shows our results where peptide to lipid ratio, (P/L), is plotted as a function of the free peptide concentration, C_f. As expected, increasing fraction of charged lipids, $\overline{\alpha}$, gives rise to a higher number of peptides bound to the bilayer. In Fig. 3.8 $\mathcal{E}_p$, the hydrophobic energy, is chosen to be $-16k_BT$ which corresponds to relatively highly hydrophobic peptides. Two sets of curves correspond to different stretching moduli, $K_a = 0.05$ and $0.1k_BT/\text{Å}^2$. Not surprisingly, over the whole range of C_f in our figure, for a given fraction of charged lipids, (P/L) is higher for the surface with lower K_a (blue lines) than for the surface with higher K_a (red lines). This is due to the smaller mechanical energy cost of penetration on the surfaces with lower stretching modulus while almost all the peptides are penetrated, $f \approx 1$, for the range of parameters selected in Fig. 3.8.

Highly hydrophobic peptides with a high net charge

In this section we present our result for highly charged peptides. The peptide charge can influence two factors: peptide-lipid attractions and peptide-image charge repulsion. The former can be dominant for surface adsorbed peptide while the later is more important for penetrated peptides. In Fig. 3.9 the peptide to lipid ratio, (P/L), and fraction of penetrated peptides, f, are plotted as a function of the free peptide concentration, C_f. In comparion with Fig. 3.8, the fractions of penetrated peptides are lower. This shows the tendecy of peptides to remain adsorbed on the surface rather than penetrating inside the bilayer. This is because of the lower energy associated with adsorption of peptides on the surface (due to stronger peptide-lipids attraction) and higher energy associated with peptide

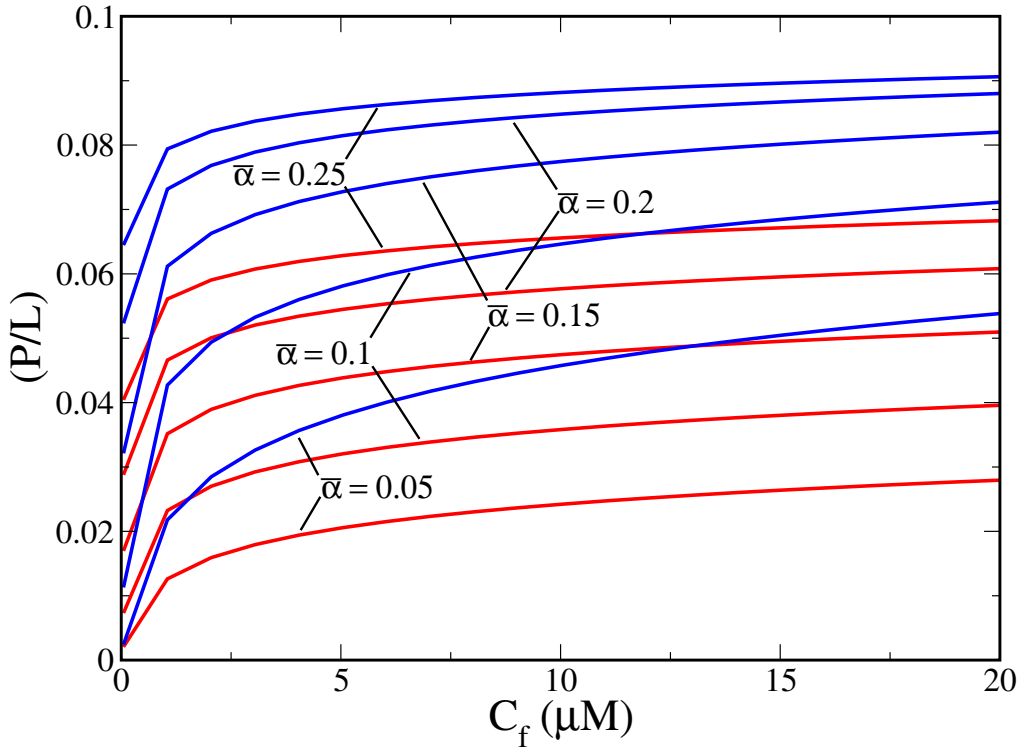

Figure 3.8: Peptide to lipid ratio as a function of the free peptide concentration, C_f. Here, $Q_p = 4$ and $\mathcal{E}_p = -16k_BT$. Surface stretching modulus si chosen as $K_a = 0.05k_BT/\text{Å}^2$ (blue lines) and $K_a = 0.1k_BT/\text{Å}^2$ (red lines). For the parameter range selected in this figure, the fraction of penetrated peptides, f, is close to one.

penetration (due to image charge-peptide repulsion).

An intersting feature of our theory emerges from Fig. 3.9 for the curves with high $\overline{\alpha}$ with $K_a = 0.05 k_B T/\text{Å}^2$. A transition is observed in the population of peptides in different states on the surface. As the concentration of the free peptides increases, peptides flip to penetrated states from surface adsorbed states. This behaviour was indeed observed in an experimental work by Binder and Lindblom in (P/L) as a function of $\overline{\alpha}$ [36].

Peptides with low hydrophobicity

Hydrophobic energy is responsible for penetration of peptides inside the bilayer. Peptides with low hydrophobicity preferentially remain adsorbed on the surface instead of penetrating inside the bilayer. In this case, increasing the fraction of charged lipids results in higher (P/L) ratio. There is, however, an optimal charge for the peptide which results in a maximum (P/L) ratio. Regarding the electrostatic energy of one single peptide on the surface, the peptide charge encourages adsoption of peptides to the bilayer. When there is a high density of peptides on the surface, higher values for the peptide charge results in stronger peptide-peptide repulsions. On the other hand, it also gives rise in larger ΔA (defined in Sec.3.3) and thus larger mechanical energy cost. As a result, there is an optimal charge for the peptide binding which depends on the fraction of charged lipids, $\overline{\alpha}$, and bulk concentration of peptides, C_f. Fig. 3.10 shows our results where $\mathcal{E}_p$ is chosen to be $-5k_BT$. The fraction of penetrated peptides calculated for the range of parameters in Fig. 3.10 is lower than 0.1, meaning that almost all of the peptides are adsorbed on the surface.

Optimal peptide charge for penetration

Penetration of the peptides is an important factor in the rupture of the membranes in Fig. 3.11. When the density of the penetrated peptides reaches a threshold value, the transient pores start to form on the bilayer which finally gives rise to rupture of the membrane.

In this section we present our results for the density of penetrated peptides. We find that for highly charged surfaces, $\overline{\alpha} \geq 0.25$, (P/L) ratio for penetrated peptides

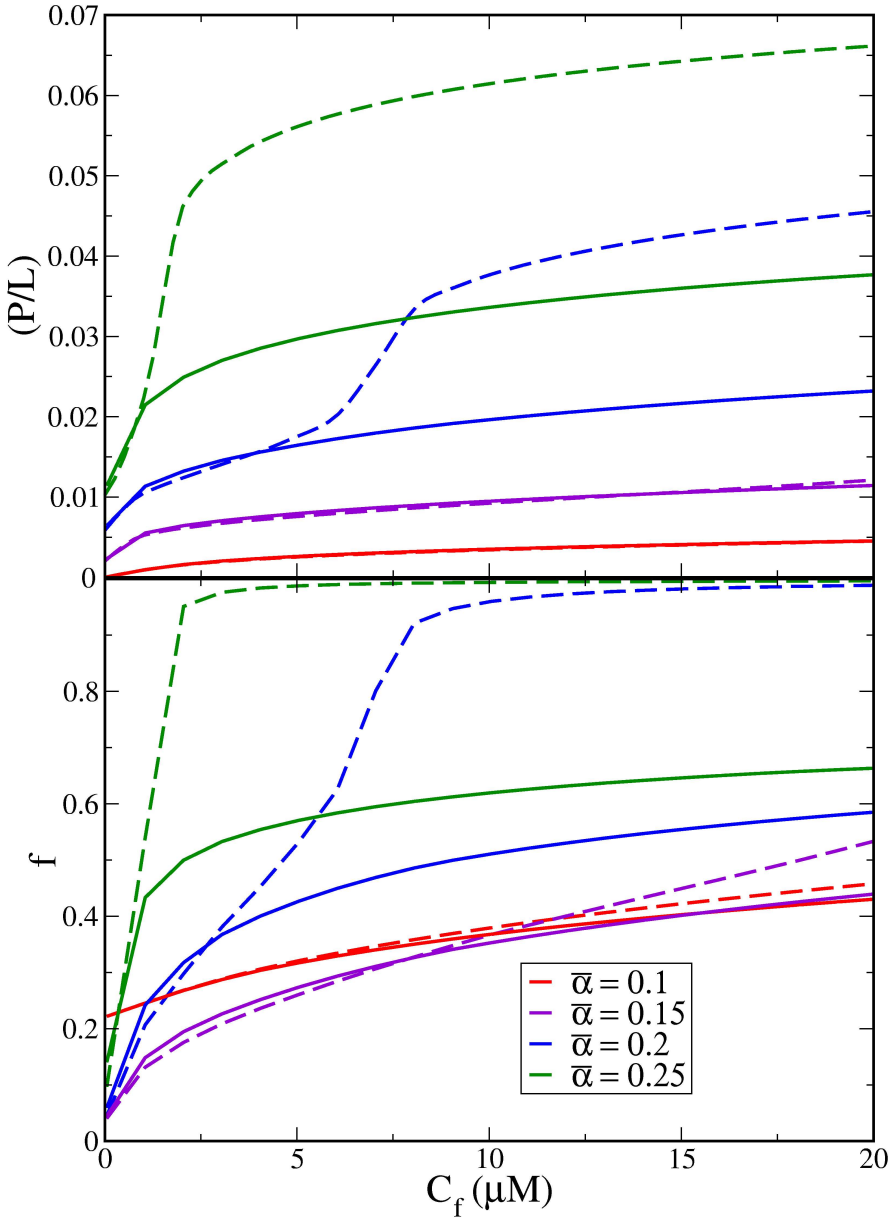

Figure 3.9: Peptide to lipid ratio (upper figure) and fraction of penetrated peptides (lower figure) as a function of the free peptide concentration, C_f, for surface stretching modulus of $K_a = 0.05 k_B T/\text{Å}^2$ (blue lines) and $K_a = 0.1 k_B T/\text{Å}^2$ (red lines). Here, $Q_p = 10$ and $\mathcal{E}_p = -16 k_B T$

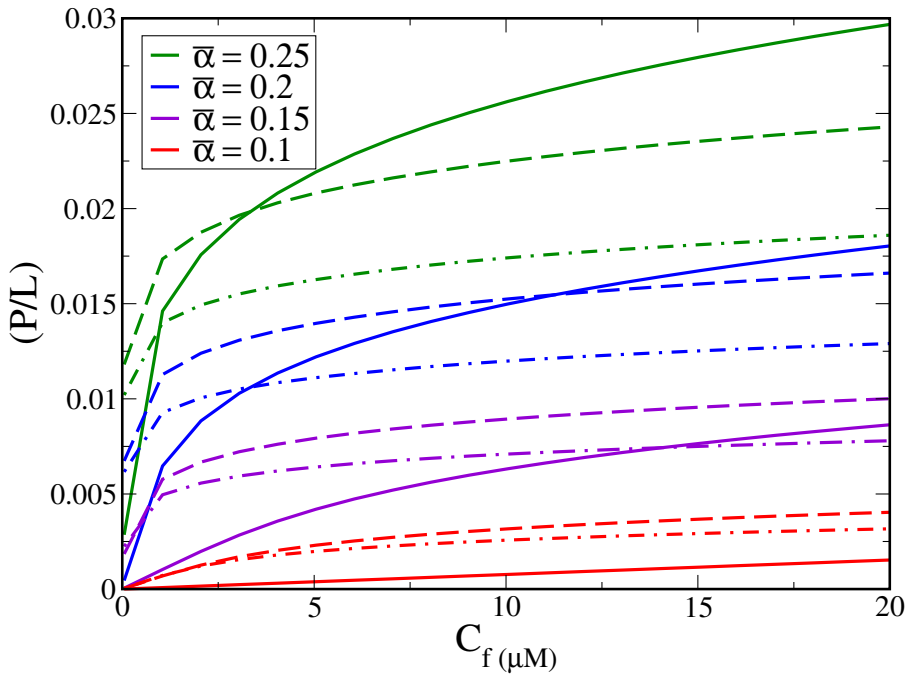

Figure 3.10: Peptide to lipid ratio as a function of the free peptide concentration, C_f. Curves are plotted for different values of peptide charge, $Q_p = 4$ (solid line), $Q_p = 7$ (dashed line) and $Q_p = 10$ (dot-dashed line). Hydrophobic energy and surface elastic modulus are chosen as $\mathcal{E}_p = -5k_BT$ and $K_a = 0.05k_BT/\text{Å}^2$.

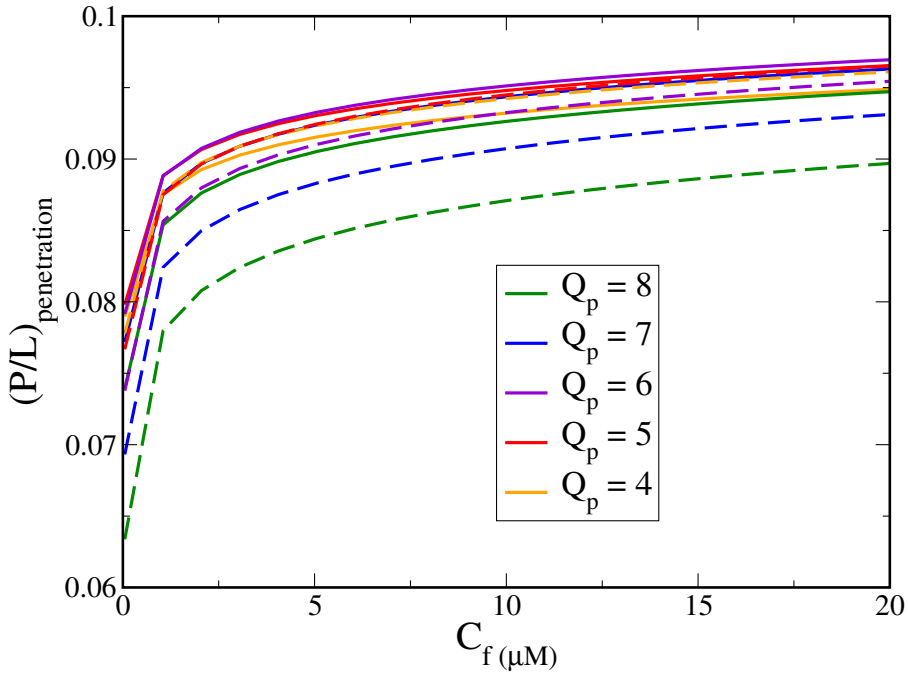

Figure 3.11: Ratio of penetrated peptides to lipids as a function of the free peptide concentration, C_f. Curves are plotted for different fractions of charged lipids, $\overline{\alpha} = 0.25$ (dashed lines) and $\overline{\alpha} = 0.3$ (solid lines). Hydrophobic energy and surface elastic modulus are chosen as $\mathcal{E}_p = -20k_BT$ and $K_a = 0.05k_BT/\text{Å}^2$.

changes non-monotonically as a function of Q_p. For $\overline{\alpha} = 0.25$ maximum penetration corresponds to $Q_p = 5$ (red dashed line in the figure) and for $\overline{\alpha} = 0.3$ the optimal peptide charge is at $Q_p = 6$ (violet solid line in the figure). This finding shows that there is an optimal charge for the peptides which can rupture the lipid bilayer.

3.5 Summary and Conclusions

In summary, we have studied theoretically the interactions of charged antimicrobial peptides with negatively charged lipid bilayers. In particular, we have calculated the density of the peptides bound to the surface of the lipid bilayer where they can be either adsorbed on the surface of the lipid bilayer or penetrated inside the head-group of the lipids. To this end, we have used a three-state model for the peptides

in which they can be in one of the states of surface adsorbed, penetrated inside the bilayer or free at bulk. The densities of the peptides in different states on the surface (at equilibrium) are found by balancing the chemical potentials of different states. In our theory, hydrophobic energy is a tuning parameter while the electrostatic and mechanical energies are calculated explicitly. We have used a hexagonal lattice model for the spatial distribution of the pepetides on the surface of the bilayer, which approximately captures the peptide-peptide interactions. Our results show that dielectric discontinuities play an important role in the penetration of a highly charged peptide inside a lipid bilayer. Due to peptide-image charge repulsions, dielectric discontinuities discourage penetration of the pepetides. On the other hand, adsorbed peptides reduce the mechanical free energy penalty for insertion by reducing the head-group area of lipids in their binding layer. The competition between mechanical energy and electrostatic energy results in an optimal charge for the penetration of peptides. Under certain conditions, the density of bound peptides changes abruptly when the surface charge density of the bilayer or the free peptide concentration is increased. Our results show that at the transition point, the fraction of penetrated peptides increases to large values (≈ 1) meaning most of bound peptides are penetrated. This finding is consistent with the experimental work by Binder and Lindblom [36].

Appendix A

In this appendix we find the area change of an elastic circular surface, reminiscent of a part of a lipid bilayer inside the WS cell described in Sec. 3.2., due to a radius dependant excess pressure (resulting from the electrostatic attraction of lipids to the peptide) attracting each part of the surface to the center. We assume that the elastic modulus of the surface, K_a, is constant over its area and does not change upon area changes. The radius of the surface is initially R. Each point of the surface is attracted to the center, the displacement of a point at distance r (from the center) due to the excess pressure is represented by $U(r)$. The area change of the surface is thus $\pi[U(R)^2 + 2RU(R)]$. The longitudinal and transverse tensions are denoted by $\gamma(r)$ and $\zeta(r)$, respectively. The area change of a differential part

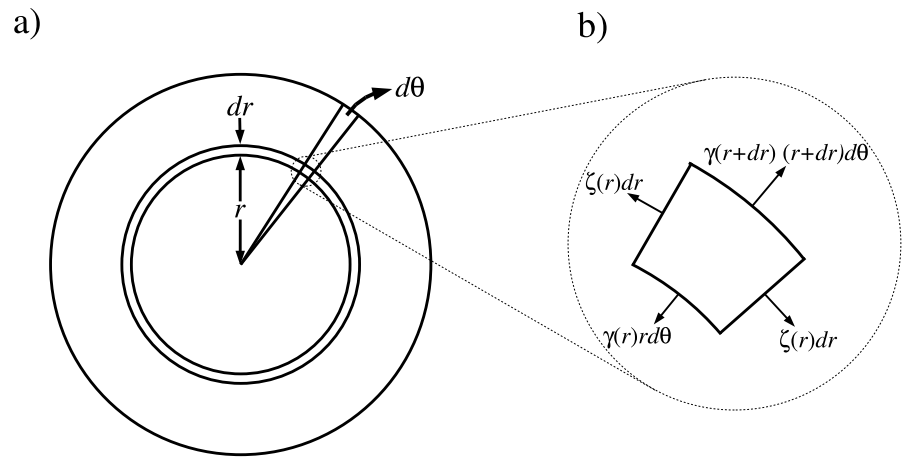

Figure 3.12: A circular elastic surface, reminiscent of a part of the lipid bilayer inside a WC cell.

of the surface (Fig. 3.12) due to the longitudinal force, $\gamma(r)rd\theta$, is $dUrd\theta$. Relating them to the elasticity of the surface we obtain

$$\frac{dU}{dr} = \frac{\gamma(r)}{K_a}, \tag{3.13}$$

where K_a is the elastic modulus of the surface. Similar equation for the area change in the transverse direction reads

$$\frac{U}{r} = \frac{\zeta(r)}{K_a}. \tag{3.14}$$

Since the differential part of the surface depicted in Fig. 3.12 is at equilibrium the resultant of the forces on this part should vanish. The force analysis on this differential part gives

$$\zeta(r) = r\frac{d\gamma}{dr} + \gamma - P(r)r, \tag{3.15}$$

where $P(r)$ is the electrostatic force per unit area of the surface at distance r from the center (this force is directed towards the center). Combining Eqs. 3.13, 3.14 and 3.15, a differential equation can be obtained for $U(r)$,

$$r^2\frac{d^2U}{dr^2} + r\frac{dU}{dr} - U = r^2\frac{P(r)}{K_a}. \tag{3.16}$$

This differential equation, subject to the boundary conditions, is solved numerically to find the area changes of the lipid bilayer when a peptide is penetrated or adsorbed on the surface of the lipid bilayer. The boundary conditions on the circumference of surface, $r = R$, arises from the fact that the tension on a free edge should be zero and thus, according to Eq. 3.13, dU/dr should vanishe at $r = R$. The other boundary condition when the peptide is penetrated (surface adsorbed) is at $r = R_p$ ($r = 0$) where $U(r = R_p) = 0$ ($U(r = 0) = 0$). ΔA^{eq} used in Sec. 3.3. is obtained as

$$\Delta A^{eq} = \pi[U(R)^2 + 2RU(R)] \tag{3.17}$$

Bibliography

[1] J.M. Berg, J.L. Tymoczko, and L. Stryer, *Biochemistry* (5th ed., New York, 2002).

[2] D. H. Boal, *Mechanics of the Cell* (Cambridge, 2002).

[3] K.M. Merz, B. Roux, *Biological Membranes* (Boston, Birkhäuser, 1996).

[4] M. Zasloff, Nature **415**, 389 (2002).

[5] B. Dreiseikelmann, Microbiol. Rev. **58(3)**,293 (1994).

[6] Antimicrobial peptides database at *http://aps.unmc.edu/AP/main.php.*

[7] G. S. Manning, J. Chem. Phys. **51**, 954 (1969).

[8] F. Oosawa, *Polyelectrolytes* (Marcel Dekker, New York, 1971).

[9] See, for example, J.-P. Hansen and H. Löwen, Annu. Rev. Phys. Chem. **51**, 209 (2000), and references therein.

[10] For the notion of a "dressed ion" in the context of electrolyte solutions, see R. Kjellander and D. J. Mitchell, J. Chem. Phys. **101**, 603 (1994).

[11] R. J. Hunter, Foundations of Colloid Science (Oxford University Press, Oxford, 2001).

[12] P. L. Felgner, Scientific American, June 102 (1997).

[13] W. M. Gelbart, R. F. Bruinsma, P. A. Pincus, and V. A. Parsegian, Physics Today, **53**(9), 38 (2000)

[14] The outer layer of a red blood cell membrane is coated with sialic acid, which is typically negatively charged. We ignore this extra complexity and assume that the outer layer is neutral.

[15] T. T. Nguyen, A. Yu. Grosberg, and B. I. Shklovskii Phys. Rev. Lett. **85**, 1568 (2000).

[16] T. T. Nguyen, A. Yu. Grosberg, and B. I. Shklovskii, J. Chem. Phys. **113**, 1110 (2000).

[17] A. Yu. Grosberg, T. T. Nguyen, and B. I. Shklovskii, Rev. Mod. Phys. **74** 329 (2002).

[18] S. Alexander, P. M. Chaikin, P. Grant, G. L. Morales, P. Pincus, and D. Hone, J. Chem. Phys. **80**, 5776 (1984).

[19] See, for example, T. Chou, M. V. Jarić, and E. D. Siggia, Biophys. J. **72**, 2042 (1997), and references therein.

[20] L. Bocquet, E. Trizac, and M. Aubouy, J. Chem. Phys. **117**, 8138 (2002).

[21] It should be noted that this equation is valid for $\kappa^{-1} \gg \ell_c$. Finite thickness of the condensed layer will further complicate u_{elec}. For $d \to \infty$ and monovalent cases, the electrostatic energy is given by $u_{elec} = 2\pi\ell_B\kappa^{-1}\sigma^{*2} + 2\pi\ell_B\ell_c\left(\frac{1}{3}\sigma_0^2 - \sigma_0\sigma_1 + \sigma_1^2\right)$. It is safe to drop the second term if $\kappa^{-1} \gg \ell_c$. For finite d, the second term will be complicated by dielectric discontinuities. Nevertheless it is conceivable that this term can easily be dominated by the first one as long as κ^{-1} is much larger than ℓ_c.

[22] R. Kjellander and S. Marcelja, Chem. Phys. Lett. **112**, 49 (1984).

[23] D. Bratko and B. Jönsson, Chem. Phys. Lett. **128**, 449 (1986).

[24] A. G. Moreira and R. R. Netz, Europhys. Lett. **57**, 911 (2002).

[25] A. Naji, S. Jungblut, A. G. Moreira, and R. R. Netz, *preprint* (2005).

[26] R. Menes, P. Pincus, and B. Stein, Phys. Rev. E **62**, 2981 (2000).

[27] R. Netz, Eur. Phys. J. E **5**, 18905 (2001).

[28] This is similar, in structure, to Eq. (2.1) in Ref. [26], which describes charge-density fluctuations at the surfaces of a bilayer. In this reference, the effective interaction was obtained for monovalent cases in the limit $\kappa \to 0$. Ours can thus be considered as a generalization of this. The correlation free energy $\mathcal{F}_{corr}$ in Eq. (2.19) obtained with this is identical to the one obtained following the Debye-Charging process. For details, see endnote [29].

[29] It is instructive to derive $\mathcal{F}_{corr}$ in Eq. (2.19) using the Debye charging process [48, 49]. Without loss of generality, we fix an ion of the ith kind and a charge $Z_i e$ at the origin $\mathbf{r}'_\perp = 0$ on the surface at $x = 0$ and consider the electric potential at $\mathbf{r}_\perp$ (denoted by $\Psi_i(\mathbf{r}_\perp, Z_i)$) due to this ion and other surrounding ions. It should be emphasized that Ψ_i is influenced by other surface charges, while $\phi(\mathbf{r}_\perp)$ is not. More precisely, Ψ_i can be obtained by integrating out all degrees of freedom associated with surface charges (and free ions) except the one at the origin. At the Debye-Hückel level, we find

$$\Psi(\mathbf{r}_\perp, Z_i) = \frac{Z_i}{e}\phi(\mathbf{r}_\perp) - \beta \sum_j \sigma_j Z_j^2 \int d\mathbf{r}'_\perp \Psi(\mathbf{r}'_\perp)\phi(\mathbf{r}'_\perp - \mathbf{r}_\perp),$$

where we dropped a contribution from a finite charge of the surface – the attraction of a counterion to the surface within the two-state model is described by Eq. (2.3). This leads to

$$\Psi(\mathbf{r}_\perp, Z_i) = \frac{Z_i}{e} \int \frac{d\mathbf{q}}{(2\pi)^2} \frac{\phi(\mathbf{q}) e^{i\mathbf{q}\cdot\mathbf{r}_\perp}}{1 + \beta \sum_j \sigma_j Z_j^2 \phi(\mathbf{q})}.$$

Following the Debye charging process [48, 49], $\mathcal{F}_{corr}$ is given by

$$\mathcal{F}_{corr} = \sum_i Z_i e \sigma_i \int_0^1 \left[\Psi(r_\perp, \zeta Z_i) - \frac{\zeta Z_i}{e}\phi(r_\perp) \right]_{r_\perp \to 0} d\zeta.$$

After the ζ-integral, this becomes the correlation free energy $\mathcal{F}_{corr}$ in Eq. (2.19). This is not a coincidence: The Debye-charging calculations and those based on the fluctuation Hamiltonian $\mathcal{H}_{corr}$ in Eq. (2.17) are at the same level. The calculations in this endnote justify (at least indirectly) the use of the fluctuation Hamiltonian $\mathcal{H}_{corr}$ in Eq. (2.17).

[30] See for example, J. Israelachvili, *Intermolecular and Surface Forces* 2nd ed. (Academic Press, 1992).

[31] A similar problem without dielectric discontinuities has been discussed by Y. W. Kim and W. Sung, *preprint* (2004).

[32] Note that the solutions in Eq. ($B.5$) are valid for $\mathbf{q} \neq 0$. In the computation of the correlation free energy in Eq. (2.19), one can truncate $\mathbf{q} \cong 0$ contributions by imposing a lower limit for the $\mathbf{q}$ integral. On the other hand, $\phi(\mathbf{q})$ obtained in Appendix B remains finite as $\mathbf{q} \to 0$. Since $d^2\mathbf{q} = 2\pi q dq$, $\mathbf{q} \cong 0$ does not contribute appreciably to the correlation free energy. Thus the lower limit can be chosen to be $\mathbf{q} = 0$ (also see the relevant discussion below Eq. (2.19)).

[33] K. Matsuzaki, Biochemical et Biophysica Acta **1462**, 1 (1999).

[34] M. Dathe, H. Nikolenko, J. Meyer, M.Beyermann, and M. Beinert, FEBS Lett. **501**, 146 (2001).

[35] Y. Shai, Biochemical et Biophysica Acta **1462**, 55 (1999).

[36] H. Binder and G. Lindblom, Biophys. J. **85**, 982 (2003).

[37] G. Drin, M. Mazel, P. Clair, D. Mathieu, M. Kaczorek, and J. Temsamani, Eur. J. Biochem. **268**, 1304 (2001).

[38] T. Wieprecht, M. Beyermann, and J. Seelig, Biochem. **38**, 10377 (1999).

[39] J. Seelig, S. Nebel, P. Ganz, and C. Bruns, Biochem. **32**, 9714 (1993).

[40] T. Wieprecht, M. Dathe, M. Beyermann, E. Krause, W. L. Maloy, Biochem. **36**, 6124 (1997).

[41] H. W. Huang, Phys. Rev. Lett. **92**, 198304 (2004).

[42] E. Kuchinka and J. Seelig, Biochem. **28**, 4216 (1989).

[43] G. Denisov, S. Wanaski, P. Luan, M. Glaser, and S. McLaughlin, Biophys. J. **74**, 731 (1998).

[44] J. G. Owicki and H. M. McConnell, Proc. Natl. Acad. Sci. **76**, 4750 (1979).

[45] T. T. Nguyen, A. Y. Grosberg, and B. I. Shklovskii, Phys. Rev. Lett. **85**, 1568 (2000).

[46] S. May, D. Harries, and A. Ben-Shaul, Biophys. J. **79**, 1747 (2000).

[47] S. Taheri-Araghi and B. Y. Ha, Phys. Rev. E **72**, 021508 (2005).

[48] D. A. Mcquarrie, Statistical Mechanics (Harper & Row, New York, 1971), Chap. 15.

[49] E. S. Velazquez and L. Blum, Physica A **244**, 453 (1997).